ELSEVIER

Palaeogeography, Palaeoclimatology, Palaeoecology 198 (2003) 69–100

PALAEO

www.elsevier.com/locate/palaeo

Magnetobiostratigraphic chronology and palaeoenvironmental history of Cenozoic sequences from ODP sites 1165 and 1166, Prydz Bay, Antarctica

Fabio Florindo [a,b,*], Steven M. Bohaty [c], Patrick S. Erwin [d], Carl Richter [e], Andrew P. Roberts [b], Patricia A. Whalen [f], Jason M. Whitehead [g]

[a] *Istituto Nazionale di Geofisica e Vulcanologia, Via di Vigna Murata 605, 00143 Rome, Italy*
[b] *School of Ocean and Earth Science, Southampton Oceanography Centre, University of Southampton, Southampton SO14 3ZH, UK*
[c] *Department of Earth Sciences, University of California, Santa Cruz, CA 95064, USA*
[d] *Department of Earth Sciences, University of Oxford, Parks Road, Oxford OX1 3PR, UK*
[e] *Ocean Drilling Program, 1000 Discovery Drive, Texas A&M Research Park, College Station, TX 77845-9547, USA*
[f] *Department of Geosciences, University of Arkansas, Fayetteville, AR 72701, USA*
[g] *Department of Geology, University of Nebraska, Lincoln, NE 68588-0340, USA*

Received 5 April 2002; accepted 3 March 2003

Abstract

A transect of three sites was drilled during Leg 188 of the Ocean Drilling Program (ODP), proximal to the East Antarctic Ice Sheet (EAIS) across the Prydz Bay continental shelf (Site 1166), slope (Site 1167), and rise (Site 1165). We present results of a palaeomagnetic and rock magnetic study of sediments recovered at sites 1165 and 1166. Magnetostratigraphic interpretations are presented for both holes and are mainly constrained by diatom and radiolarian biostratigraphies, interpreted in the light of recent refinements to Southern Ocean zonal schemes and datum calibrations for these microfossil groups. Site 1165 records a history of sedimentation on the continental rise extending back to earliest Miocene times (about 22 Ma). Several long-term changes characterise this record, including an overall trend of decreasing sedimentation rates from the bottom to the top of the hole. There is a progressive decrease in the sedimentation rate above about 308 mbsf (meters below sea floor), which is marked by a transition from dark-grey fissile claystones to greenish-grey diatom-bearing clays. At this transition, ice-rafted debris, sand grains, and total clay content also increase. The chronology presented here indicates a middle Miocene age ($\sim$14.3 Ma) for the lithological transition. Correlation to ODP Hole 747A from the Kerguelen Plateau suggests that this lithological transition coincides with the base of the Mi-3/3a $\delta^{18}O$ event, which suggests palaeoclimatic control on middle Miocene sedimentation changes at Site 1165. Core recovery was poor at Site 1166. Consequently, the magnetostratigraphic data are of limited value. The deepest cores recovered at Site 1166 record brief intervals in the early history of the EAIS for the Prydz Bay region, extending back through the early stage of glaciation to pre-glacial times. An Early Cretaceous fluvio-lacustrine unit, lagoonal deposits and sandy fluvio-deltaic units of mid–late Eocene age contain a sporadic record of the transition from humid and mild conditions to cool temperate conditions.

Keywords: magnetostratigraphy; biostratigraphy; Prydz Bay; Antarctica; Ocean Drilling Program; 1165; 1166

* Corresponding author. Tel.: +39-06-51860383; Fax: +39-06-51860397. *E-mail address:* florindo@ingv.it (F. Florindo).

0031-0182/03/$ – see front matter © 2003 Elsevier B.V. All rights reserved.
doi:10.1016/S0031-0182(03)00395-X

1. Introduction

Glaciation of the Antarctic continent, as well as the shift from warmer to colder conditions near the Eocene–Oligocene (E–O) boundary (Prothero, 1994), marks one of the most fundamental reorganisations of the global climate system in the Cenozoic. Our understanding of the timing and style of Antarctic glaciation since the late Eocene and the impact of glacial fluctuations on global sea level has largely been deduced from: (1) oceanic proxy records, including distal marine oxygen isotope and trace element records (e.g., Shackleton and Kennett, 1975; Lear et al., 2000; Zachos et al., 2001), (2) records of detrital material from the continent (e.g., Ehrmann, 1991), (3) outcrops in ice-free areas on the continent (e.g., Hambrey and McKelvey, 2000; McKelvey et al., 2001), and (4) drilling campaigns in and around the Antarctic margin (e.g., Barron et al., 1991). During the last three decades, studies of sedimentary sequences cored from the Antarctic margin and surrounding ocean basins (Deep Sea Drilling Project and Ocean Drilling Program (ODP) legs, Dry Valley Drilling Project, McMurdo Sound Sediment and Tectonic Studies, Cenozoic Investigations in the Ross Sea and Cape Roberts projects) have led to significant advances in our understanding of Antarctic glacial history.

In this paper, we present results from ODP Leg 188 (O'Brien et al., 2001), which was designed to build on the results of Leg 119 from Prydz Bay (Barron et al., 1989, 1991) by investigating the history of the Lambert Glacier–Amery Ice Shelf system during key periods of the Cenozoic (e.g., E–O boundary, Oligocene–Miocene boundary, mid-Miocene transition). During Leg 188, a transect of three sites was drilled across the Prydz Bay continental shelf (Site 1166), slope (Site 1167), and rise (Site 1165). These sites provide a proximal history of the EAIS, including the transition from East Antarctic pre-glacial to glacial conditions on the shelf (Site 1166), the number and timing of late Neogene ice expansions to the shelf edge (Site 1167) and the long-term early to late Miocene, and late Pliocene (Webb and Harwood, 1991; Harwood et al., 1992; Moriwaki et al., 1992; Wilson, 1995) transitions from temperate glacial climates to cold-climate glaciation, with superimposed short-term glacial fluctuations since early Miocene time (Site 1165) (O'Brien et al., 2001).

In this paper, we present a magnetostratigraphic study of sediments recovered at sites 1165 and 1166, together with analyses of variations in composition, concentration and grain-size of magnetic minerals throughout the drilled sequences. Our magnetostratigraphic interpretations are mainly constrained by diatom and radiolarian biostratigraphic zonations. These zonations reflect recent refinements to Southern Ocean zonal schemes and datum calibrations for these microfossil groups and are correlated to the geomagnetic polarity time scale (GPTS) of Cande and Kent (1995) and Berggren et al. (1995). We also explore the implications of our work for Antarctic glacial history by comparing the data from Leg 188 with those from ODP legs (119 and 120).

2. Regional geological setting and lithostratigraphy

Prydz Bay is a prominent re-entrant in the East Antarctic coastline between 70°E and 79°E, in the Indian Ocean sector of the Antarctic margin (Fig. 1). It lies at the downstream end of the Lambert Glacier–Amery Ice Shelf drainage system, which is the largest single ice stream flowing from the interior of the Antarctic Plateau. The Lambert Glacier drains more than 20% of the East Antarctic Ice Sheet (EAIS) (Hambrey and Dowdeswell, 1994), including the 3000-m-high Gamburtsev Subglacial Highlands, an area where, if present in the Palaeogene, some models of ice sheet growth suggest that the EAIS first developed (e.g., Huybrechts, 1993). Early glaciers would have delivered sediment into Prydz Bay and later expansion of ice sheets would have resulted in the advance of glaciers into the bay, making it an ideal place to detect the earliest Cenozoic glacial sediments on the Antarctic continental shelf.

The Lambert Glacier–Amery Ice Shelf drainage system follows the line of the Lambert Graben, which is a deep crustal structure that extends about 600 km inland, and contains several kilometers of sediment, as suggested by gravity, mag-

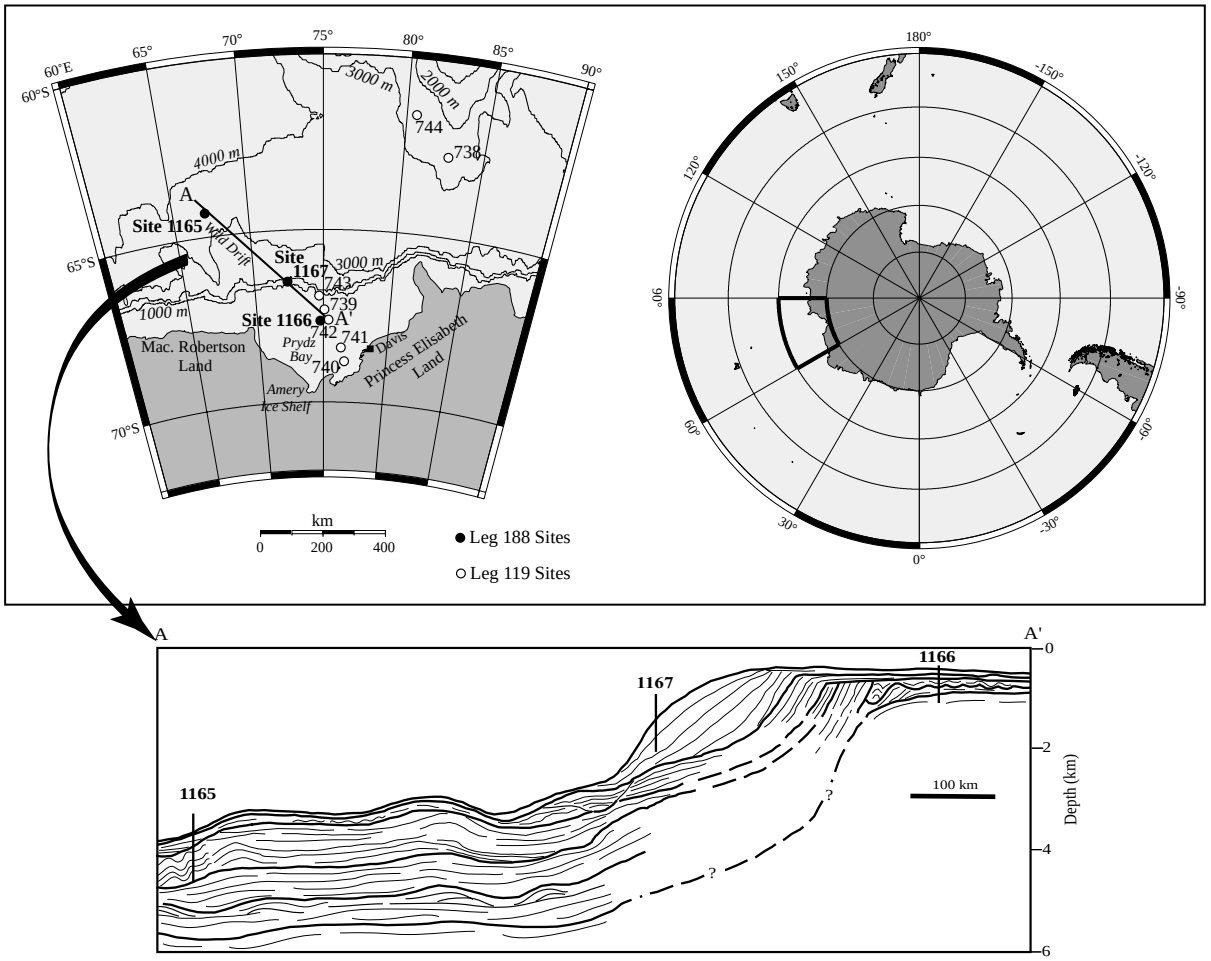

Fig. 1. Location map of Prydz Bay, with ODP sites from legs 119 and 188, and a schematic seismic section (A–A′) through the Leg 188 sites (from Cooper et al., 2001).

netic and seismic refraction data (Fedorov et al., 1982; Stagg, 1985; Cooper et al., 1991). The graben is part of a major structure which has been interpreted as the failed arm of a triple junction that developed as a consequence of break-up of East Antarctica and India during the Early Cretaceous (Stagg, 1985; Chand et al., 2001; Lawver et al., 1991, 1992; Lawver and Gahagan, 2001).

Uplifted Cenozoic glacial–marine strata of the Pagodroma Group occur throughout the Prince Charles Mountains, flanking the western margin of the Lambert Graben (Hambrey and McKelvey, 2000; McKelvey et al., 2001), and were deposited up to 600 km inland from the current Amery Ice Shelf edge (Whitehead et al., 2000). Temperate terrestrial glacigene sediments also crop out 750 km inland (Whitehead and McKelvey, in press), and provide the most southerly Cenozoic record within the Lambert Graben. The sedimentary sequences that fill the Prydz Bay Basin in the outer Lambert Graben (Stagg, 1985) were partially drilled during ODP Leg 119, at sites 740 and 741 (Fig. 1). The Prydz Bay Basin is separated from the sediment underlying the outer shelf, slope, and rise by a northeast-plunging basement ridge that extends from the southwestern corner of Prydz Bay.

ODP Site 1165 (64°22′S, 67°13′E) was drilled

on the continental rise offshore from Prydz Bay on a large sediment drift (the Wild Drift) at a water depth of 3537 m in order to provide a record of sedimentation that extends back to the onset of contour current-influenced deposition on the continental rise. Drilling at this site yielded a relatively continuous 999-m-thick sedimentary section, currently the deepest rock-hole drilled on the Antarctic margin. The recovered section consists of three primary lithostratigraphic units (Fig. 2). The uppermost Unit I (from 0 to 63.8 m below sea floor (mbsf)) consists of brown diatom clay with minor diatom-bearing green clay that contains dispersed lonestones. The underlying Unit II (from 63.8 to 307.8 mbsf) is composed of structureless greenish-grey diatom clay interbedded with dark-grey diatom-bearing clay. The uppermost and lower parts of this unit contain dispersed sand grains, granules, and lonestones. Unit III (from 307.8 to 999.1 mbsf) consists of dark-grey, thinly bedded, planar-laminated claystones interbedded with thin greenish-grey bioturbated massive claystone with rare dispersed sand grains, granules, and lonestones (O'Brien et al., 2001).

ODP Site 1166 (67°42′S, 74°47′E) was drilled on the Prydz Bay continental shelf about 40 km southwest of ODP Site 742 (Barron et al., 1989, 1991) at a water depth of 486 m (Fig. 1). This site was selected to sample earliest Cenozoic glacial sediment, to date the onset of Antarctic glaciation and to document changes in palaeoenvironments and biota that accompanied the onset of glaciation. At Site 1166, a 381.3-m section was recovered, which consists of poorly sorted, sandy and fine-grained sediments, with core recovery of about 19% (Fig. 2). Integration of down-hole logging data (Formation MicroScanner resistivity images) and sedimentological descriptions of the recovered core material permitted interpretation of lithology and rock properties in intervals where core recovery was low (Barr et al., 2001; O'Brien et al., 2001).

Five lithostratigraphic units were recognised by O'Brien et al. (2001) at site 1166. The uppermost unit, from the sea floor to 135.41 mbsf, is composed of poorly sorted sediments with dispersed lonestones, similar to those sampled at Site 742. Unit II (135.63–156.62 mbsf) is composed of claystone and diatom-bearing claystone with interbedded sands and lonestones. Unit III (156.62–267.17 mbsf) is characterised by massive and deformed sands with a silty-clay matrix. The lower part of this unit is rich in organic material, including pieces of wood. Unit IV (276.44–314.91 mbsf) comprises carbonaceous clay and fine sandy silt with organic-rich laminae. Unit V (342.80–342.96 mbsf) consists of finely laminated grey claystone.

3. Laboratory procedures

The bulk of the remanence measurements made during Leg 188 were carried out using a 2-G Enterprises (model 760-R) pass-through cryogenic magnetometer equipped with pick-up coils which enable measurement of the magnetic signal over an interval of ~8 cm (Shipboard Scientific Party, 2001a). The natural remanent magnetisation (NRM) was routinely measured before and after alternating field (AF) demagnetisation on all archive-half core sections at 4-cm intervals. Time constraints permitted analysis with only 2 or 3 AF demagnetisation steps at 10, 20 and 30 mT peak values for most of the core sections. The low-maximum-peak AFs ensured that the archive halves remained useful for shore-based palaeomagnetic studies. In a few intervals, the presence of strong magnetic overprints necessitated progressive demagnetisation of the archive halves up to 60–80 mT. Measurements at the end of each core section, and those within intervals of drilling-related core deformation and in the vicinity of obvious metamorphic and/or igneous pebbles, were removed during data processing.

Discrete samples (standard 8-cm^3 plastic cubes) were collected from the working halves of the cores at c. 1-m intervals and were analysed to verify the reliability of the whole-core measurements on the archive core halves. If possible, these samples were taken from fine-grained horizons and sampling was adjusted to avoid intervals with drilling-related core deformation and pebbles. Most discrete samples were AF demagnetised at 10, 20, 30, 40, 50, 60, 70, and 80 mT using

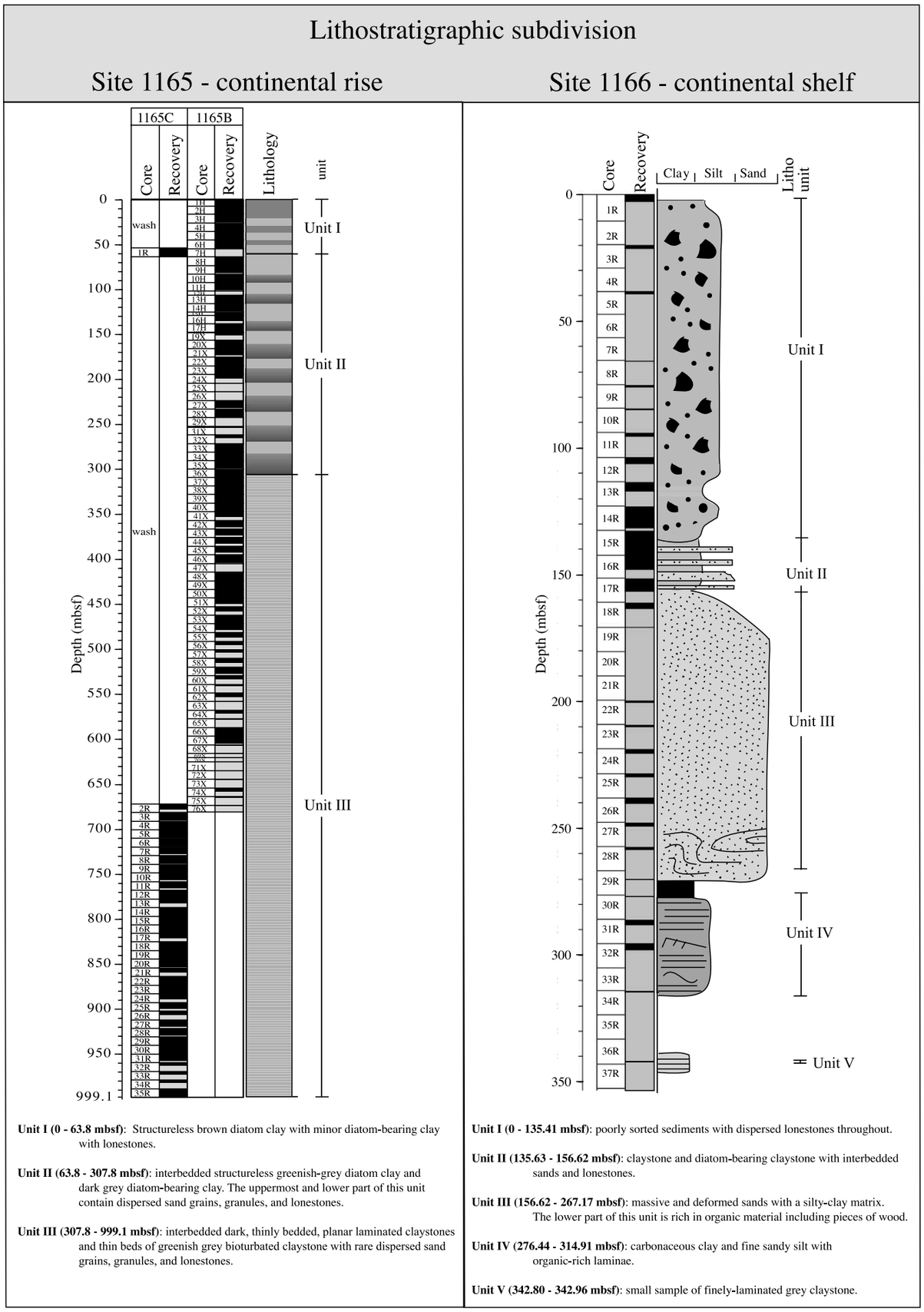

Fig. 2. Lithostratigraphic columns (after O'Brien et al., 2001) for ODP sites 1165 and 1166.

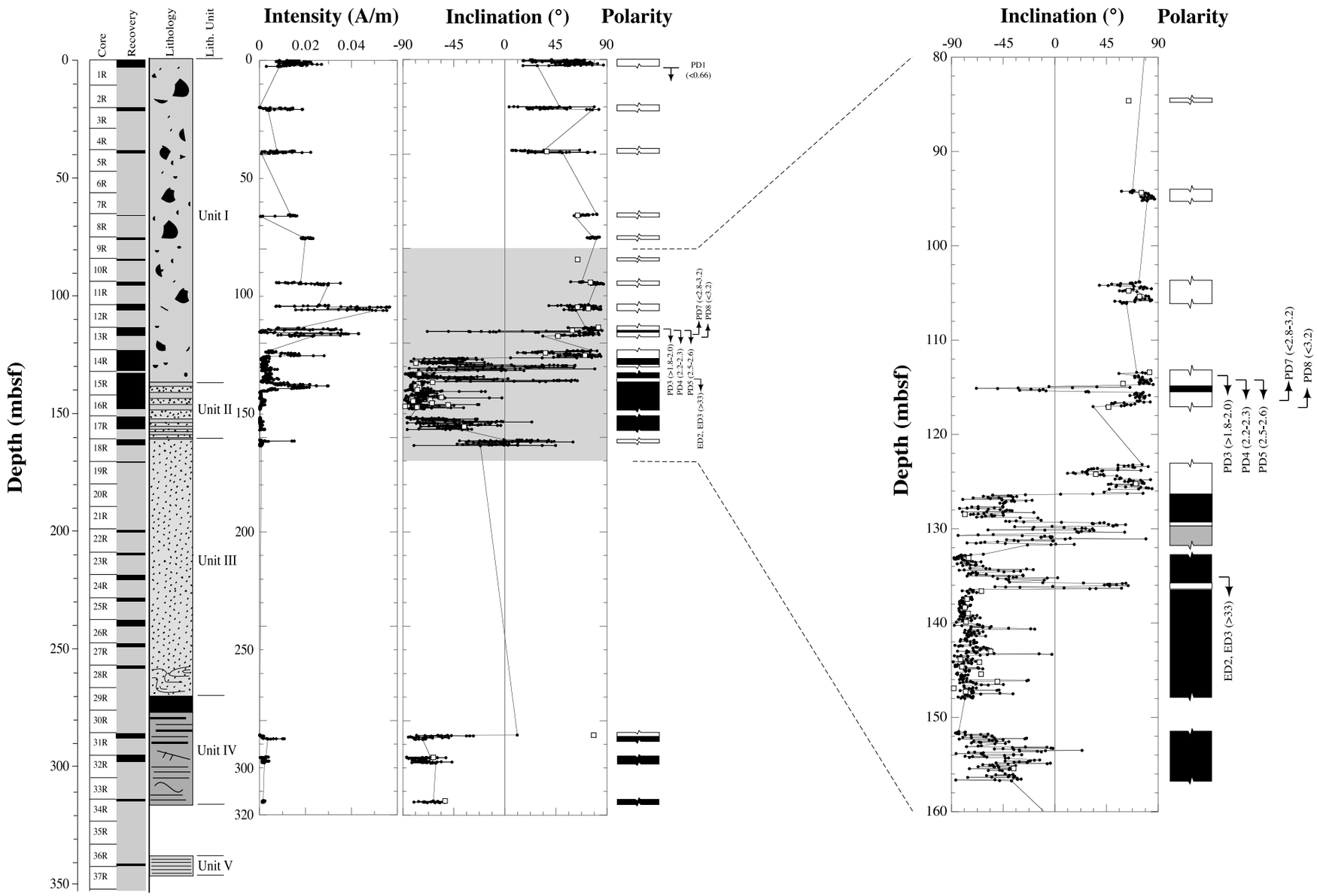

Fig. 13. Lithostratigraphic column and magnetostratigraphic record, including plots of NRM intensity, palaeomagnetic inclination after demagnetisation of the split core at 30 mT, and an enlargement of the polarity data for the interval between 80 and 160 mbsf, for Hole 1166A (0–320 mbsf). Inclinations for ChRM data from discrete samples are shown as open squares on the inclination plot. Polarity is shown on the log to the right. Black (white) = normal (reversed) polarity intervals and shading indicates intervals with no core recovery.

the in-line demagnetiser installed on the 2-G Enterprises pass-through cryogenic magnetometer on the ship. A subset of samples was thermally demagnetised using a Schonstedt TSD-1 oven on the ship. All of the samples subjected to thermal demagnetisation were measured at steps of 20, 100, 200, 300, 330, 360, 400, 500, 550, 600, 650, and 700°C. The magnetic susceptibility was measured after each heating step to monitor for thermal alteration of magnetic minerals.

The lack of azimuthal orientation for these cores did not pose a problem for determination of palaeomagnetic polarity in our magnetostratigraphic studies because the geomagnetic field at the latitude of sites 1165 (64.4°S) and 1166 (64.7°S) has a steep inclination (±76.5° and ±76.7°, respectively, assuming a geocentric axial dipole (GAD) field). The palaeomagnetic inclinations were determined using the 20–30-mT steps from the long-core measurements and using principal component analysis (Kirschvink, 1980) for data from multiple demagnetisation steps for dis-

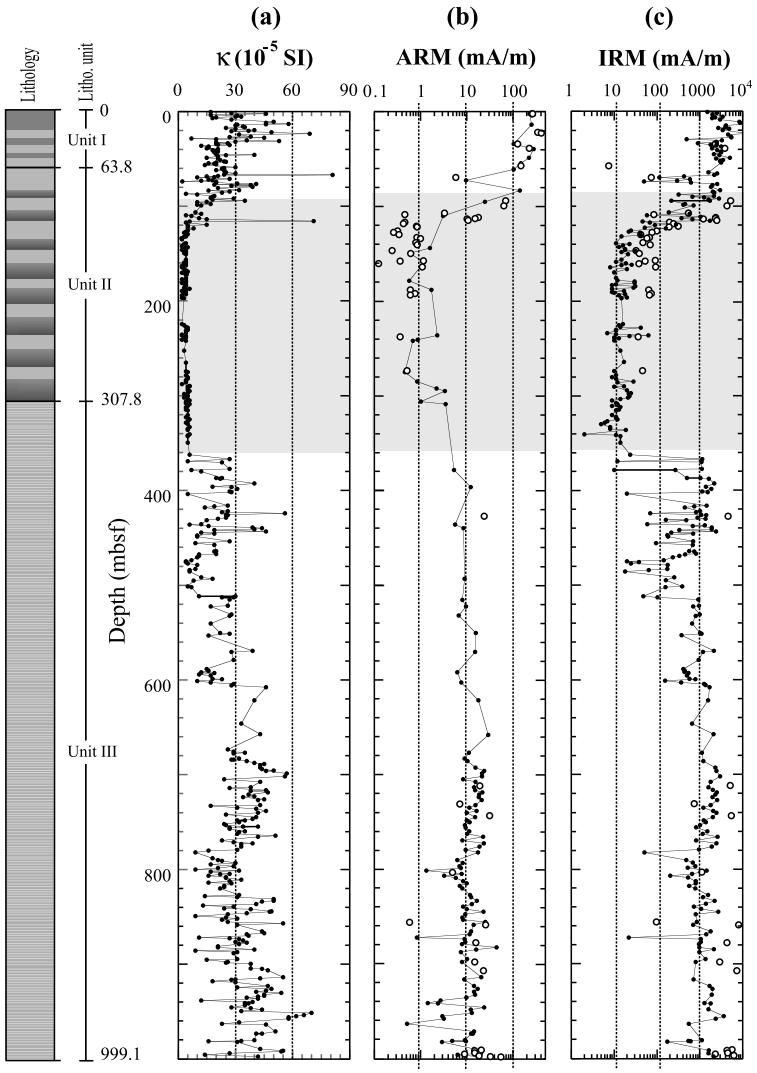

Fig. 3. Lithostratigraphic column and down-core variations of low-field magnetic susceptibility (κ), ARM and IRM for Site 1165.

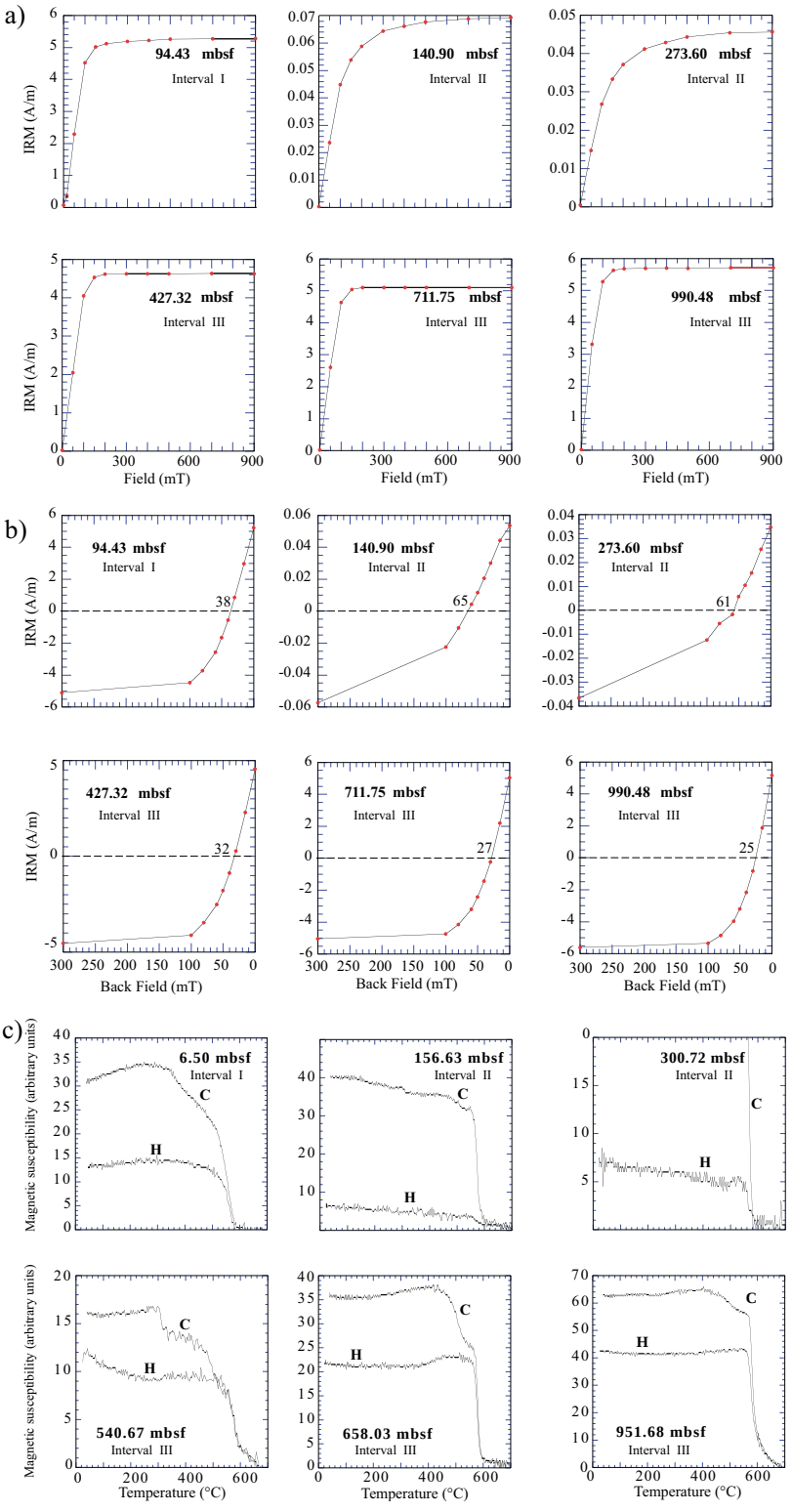
a)
IRM (A/m)
94.43 mbsf
Interval I
140.90 mbsf
Interval II
273.60 mbsf
Interval II
427.32 mbsf
Interval III
711.75 mbsf
Interval III
990.48 mbsf
Interval III
Field (mT)
b)
IRM (A/m)
94.43 mbsf
Interval I
38
140.90 mbsf
Interval II
65
273.60 mbsf
Interval II
61
427.32 mbsf
Interval III
32
711.75 mbsf
Interval III
27
990.48 mbsf
Interval III
25
Back Field (mT)
c)
Magnetic susceptibility (arbitrary units)
6.50 mbsf
Interval I
156.63 mbsf
Interval II
300.72 mbsf
Interval II
540.67 mbsf
Interval III
658.03 mbsf
Interval III
951.68 mbsf
Interval III
C
H
Temperature (°C)

crete samples. The maximum angular deviation (MAD) was calculated to provide an estimate of the precision for each best-fit line. Samples were only included in this study if MAD values were less than 10°.

Mineral magnetic analyses were conducted on a set of representative discrete samples after they had been subjected to AF demagnetisation in order to estimate down-core variations in the composition, concentration and grain-size of magnetic minerals. Low-field magnetic susceptibility (κ) was routinely measured for all the discrete samples using a Bartington Instruments MS2 magnetic susceptibility meter. Further analyses were made on a selected subset of discrete samples. These analyses included: (1) stepwise acquisition of an isothermal remanent magnetisation (IRM) in fields up to 1.3 T; (2) determination of the coercivity of remanence (B_{cr}) and *S*-ratio ($-IRM_{-0.3T}/IRM_{1.3T}$) by progressively applying increasing back-fields up to 300 mT after application of a forward field IRM at 1.3 T; and (3) anhysteretic remanent magnetisations (ARMs) imparted with a 100 mT AF and a 0.05 mT DC bias field. For a few samples, we also carried out a stepwise thermal demagnetisation of a composite IRM (Lowrie, 1990) at steps of 20, 100, 200, 300, 330, 360, 400, 500, 550, 600, 650, and 700°C. Fields of 1.3, 0.5, and 0.12 T were applied along the *x*, *y*, and *z* axes of samples to distinguish between high-, intermediate-, and low-coercivity magnetic phases, respectively. The temperature dependence of magnetic susceptibility was also measured for selected samples from room temperature up to 700°C, using a furnace-equipped Kappabridge KLY-3 magnetic susceptibility meter (Hrouda, 1994).

4. Results

4.1. Rock magnetism – ODP Site 1165

Based on magnetic properties, the drilled sedimentary sequence at Site 1165 can be divided into three main rock magnetic intervals that are not clearly associated with lithological variations (Fig. 3). Throughout the sequence, down-core variations of κ are associated with similar changes in ARM and IRM intensity. The highest values of these parameters occur in the interval from 0 to ~ 120 mbsf (Rock Magnetic Interval I) and below 365 mbsf (Rock Magnetic Interval III). Within Rock Magnetic Interval II, between ~120 and 365 mbsf, κ decreases to extremely low values. These rock magnetic parameters indicate that the concentration of magnetic grains varied by more than one order of magnitude between Rock Magnetic Interval II and Intervals I and III.

The rock magnetic zonation for Site 1165 also reflects differences in the composition of the magnetic minerals. Within Rock Magnetic Intervals I and III, several lines of evidence indicate that magnetite is the main magnetic mineral. More than 90% of the saturation IRM is reached in fields of 200–300 mT (Fig. 4a) and B_{cr} ranges between 25 and 38 mT (Fig. 4b). The magnetic susceptibility decreases near 580°C upon heating, which indicates that magnetite is the major contributor to the susceptibility (Fig. 4c). The observed increases in κ during heating are probably due to the thermally induced growth of new magnetite from iron-bearing clays. Within Rock Magnetic Interval II, the IRM is not saturated at fields above 500 mT and B_{cr} values range between 61 and 65 mT. Temperature-dependent κ curves undergo a change in slope close to 580°C, but, in addition, for samples from Rock Magnetic Interval II and parts of Rock Magnetic Interval III, there is a residual κ between 560 and 680°C. These data confirm the presence of magnetite within Rock Magnetic Intervals II and III, which occurs along with variable amounts of hematite.

4.2. Palaeomagnetic behaviour – ODP Site 1165

The interval with decreased abundance of ferrimagnetic minerals between ~120 and 365 mbsf

Fig. 4. Selected rock magnetic results for Site 1165. (a) Stepwise IRM acquisition curves, (b) curves of back-field demagnetisation of the IRM (numbers denote the coercivity of remanence, B_{cr}), and (c) temperature dependence of magnetic susceptibility. The roman numerals relate to rock magnetic intervals (see text). H = heating, C = cooling.

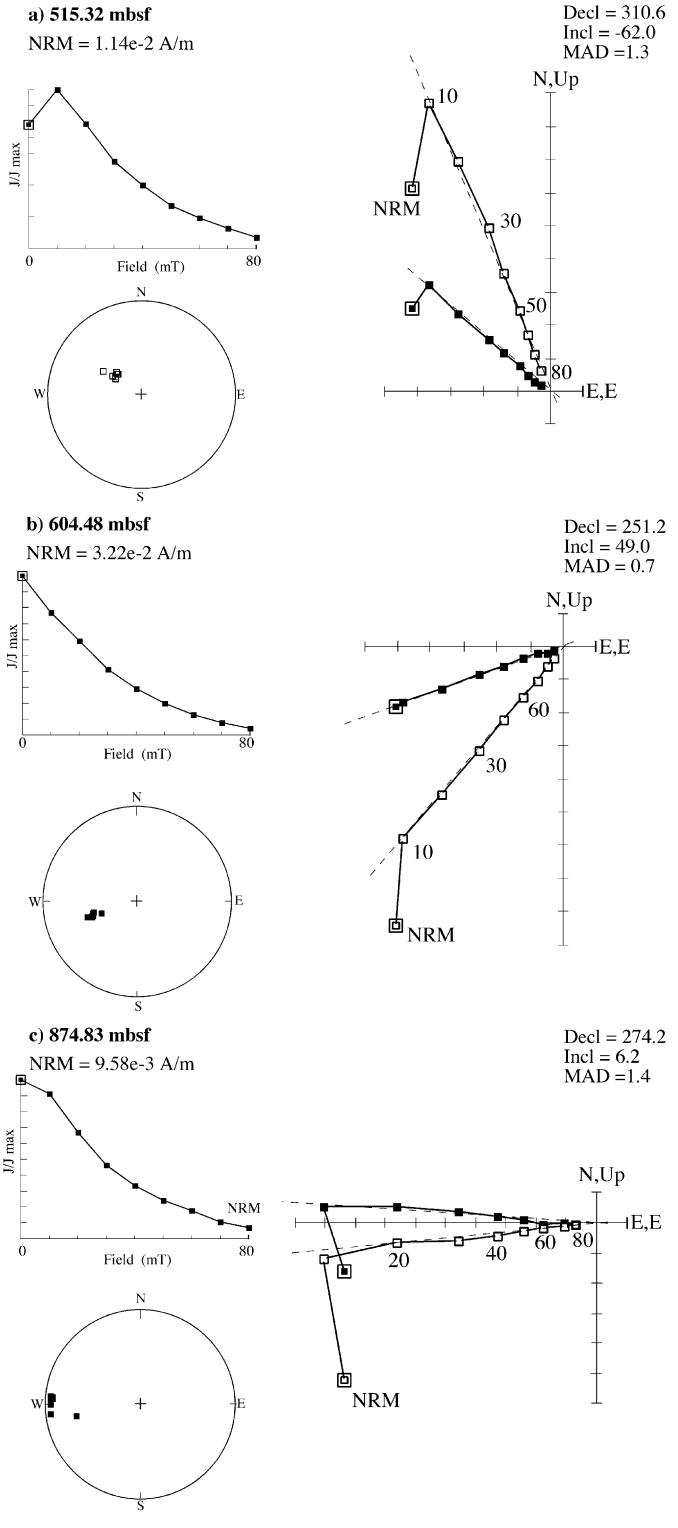
a) 515.32 mbsf
NRM = 1.14e-2 A/m
Decl = 310.6
Incl = -62.0
MAD =1.3
J/J max
0
Field (mT)
80
N
W
E
S
N,Up
10
NRM
30
50
80
E,E
b) 604.48 mbsf
NRM = 3.22e-2 A/m
Decl = 251.2
Incl = 49.0
MAD = 0.7
J/J max
0
Field (mT)
80
N
W
E
S
N,Up
E,E
60
30
10
NRM
c) 874.83 mbsf
NRM = 9.58e-3 A/m
Decl = 274.2
Incl = 6.2
MAD =1.4
J/J max
NRM
0
Field (mT)
80
N
W
E
S
N,Up
E,E
20
40
60
80
NRM

(Fig. 3) is dominated by weak and unstable magnetisations. With the exception of this interval, most of the samples from sites 1165 and 1166 are affected by a steep reversed polarity overprint. This overprint appears to be drilling induced. Such overprints are common in drill cores and have been routinely observed in recovered ODP sediments (e.g., Fuller et al., 1998). In many cases, the overprints reported in the literature have normal polarity, but consistent reversed polarity overprints have also been observed in some ODP cores (e.g., Weeks et al., 1995). For Leg 188 cores, this magnetic overprint was successfully removed at peak fields of 10 mT and a stable characteristic remanent magnetisation (ChRM) is evident for a large proportion of the analysed samples (Fig. 5a,b). The consistently steep, downward orientation provided unambiguous evidence that neither the core nor the samples were mistakenly inverted at any stage. In a few cases (i.e., samples between 860 and 880 mbsf), an additional overprint, which could only be partially removed even after demagnetisation at peak fields of 60–80 mT, is present. This overprint has a nearly horizontal inclination (Fig. 5c), and, in most cases, is parallel to the split-plane of the core (i.e., in sample coordinates, the overprint is in the y–z plane with $x = 0$); in a few cases, the overprint is perpendicular to the split-plane (in the x–z plane with $y = 0$). In other drillcores, two mechanisms have been suggested to explain this type of overprint: (1) a radial overprint as documented by Fuller et al. (1998), which is related to strong magnetic fields in the cutting-shoe and/or core barrel, and (2) a core-splitting overprint (Wilson et al., 2000; Florindo et al., 2001). At this stage, we have not determined which of the two suggested mechanisms is responsible for the overprint.

An inclination histogram for Rock Magnetic Interval I illustrates the dominance of the steep reversed polarity overprint before demagnetisation (Fig. 6a). After demagnetisation at 20 mT, this secondary component is removed and a clear bimodal ChRM distribution is isolated, which demonstrates the presence of two stable polarity states (Fig. 6b). The two statistical modes are slightly shallower than would be expected ($\pm 76.5°$) for the latitude at Site 1165 (assuming a GAD field). There is no evidence for stratal tilt in the sediments recovered at Site 1165. The inclination shallowing is therefore probably related to the inclination error that arises from the physical rotation of detrital grains toward the bedding plane, which is commonly observed in sediments that have undergone significant compaction after deposition (e.g., Anson and Kodama, 1987; Arason and Levi, 1990) and where bioturbation is limited or absent (Verosub, 1977).

4.3. Magnetic polarity zonation – ODP Site 1165

The clear bimodal distribution of normal and reversed polarity palaeomagnetic directions (Fig. 6b) suggests that the magnetostratigraphic signal identified for Site 1165 is robust. Within Rock Magnetic Interval I, there is a clear magnetostratigraphic signal down to about 90 mbsf (Fig. 7). In this interval, 122 discrete samples were analysed in addition to the measurements made on the split core. Agreement between these two types of data is good (Fig. 7), which also suggests that the magnetostratigraphic signal is reliable.

In the lower part of Rock Magnetic Interval I (below 90 mbsf) and in Rock Magnetic Interval II, magnetisations are generally weak and no palaeomagnetic interpretation is attempted. The only constraints on the age interpretation for this part of Site 1165 are based on diatom and radiolarian biostratigraphies (Fig. 8). Magnetisations are much stronger and more stable in Rock

Fig. 5. AF demagnetisation behaviour for three representative samples from Site 1165. For the vector component diagrams, open (closed) symbols represent projections onto the vertical (horizontal) plane. The dashed lines represent linear regression fits that indicate the ChRM direction for each sample. The stereoplots are equal area stereographic projections, where solid (open) symbols represent lower (upper) hemisphere projections. Samples are not azimuthally oriented and declinations are reported in the laboratory coordinate system with respect to the split face of the drill-core. J = NRM intensity. MAD = maximum angular deviation for the ChRM determination.

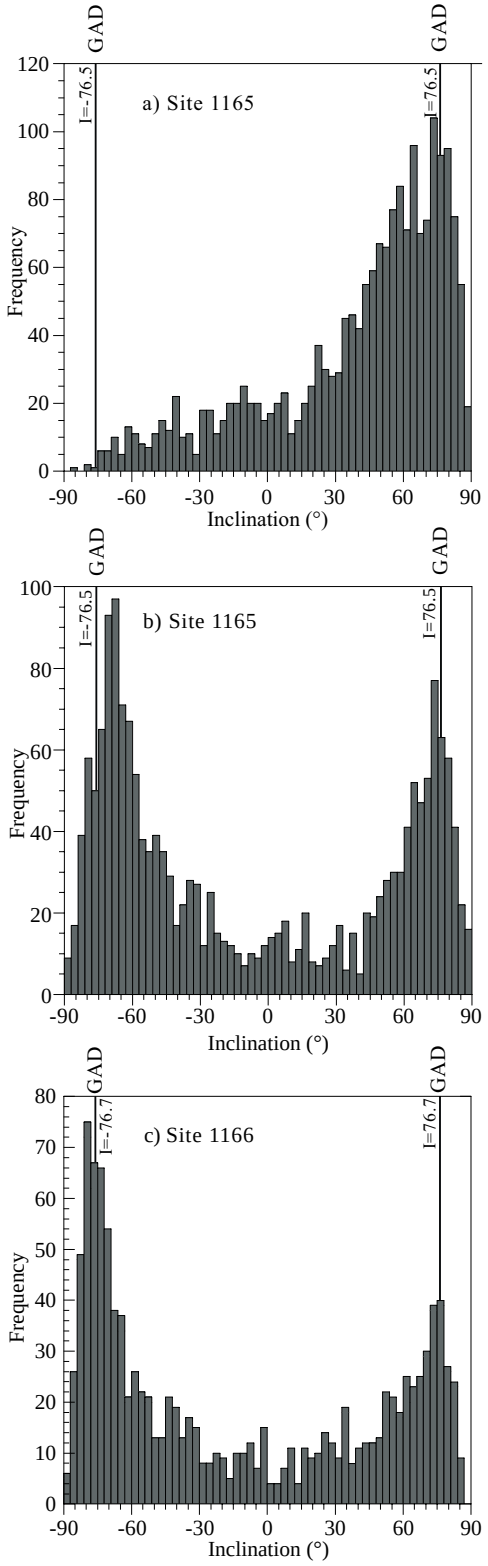

Magnetic Interval III, where it is possible to provide palaeomagnetic constraints on the chronostratigraphic interpretation despite poorer core recovery. This lower part of the record was recovered using extended core barrel (XCB) drilling. Visual inspection of down-hole variations in palaeomagnetic directions (Fig. 9) indicates that the signal is not as clear as in the upper 90 mbsf, where advanced piston coring was used. Some of the high-frequency palaeomagnetic fluctuations probably result from the presence of clasts and/or coarse-grained intervals and do not represent geomagnetic field behaviour (Figs. 7 and 9). Care was taken when interpreting the palaeomagnetic signal from such intervals. Deformation resulting from XCB drilling is also probably partially responsible for the greater noise in the palaeomagnetic signal in the lower part of the hole. Discrete samples were taken from undisturbed parts of the core; data from such samples confirm the overall polarity pattern (Fig. 9) and give confidence in the split-core results despite the possibility that these results are partially affected by drilling-related deformation. Magnetostratigraphic interpretations are presented in Section 5.

4.4. Rock magnetism – ODP Site 1166

Despite poor core recovery in Hole 1166A (about 19%), enough sediment was recovered to establish a low-resolution rock magnetic stratigraphy for the sequence. Down-hole variations of κ and ARM and IRM intensities are shown alongside lithology in Fig. 10. The highest concentrations of magnetic minerals occur in the glacially influenced sediments of Lithostratigraphic Unit I. Thermal demagnetisation of three-axis IRMs indicates that most of the remanence is held by the low-coercivity fraction (Fig. 11). Above ~140 mbsf, the IRM undergoes a large decrease between 330 and 360°C and then gradually decays

Fig. 6. Histograms of palaeomagnetic inclinations from discrete samples and long-core measurements for: (a) Site 1165 prior to AF demagnetisation, (b) Site 1165 after AF demagnetisation at 20 mT, and (c) Site 1166 after AF demagnetisation at 20 mT. The expected inclinations are shown for the respective site latitudes (assuming a GAD field).

to near-zero values between 550 and 600°C (Fig. 11). The bulk magnetic susceptibility progressively decreases during heating from 20 to 700°C. Below ~140 mbsf, the IRM is almost completely demagnetised between 330 and 360°C, at which point the bulk susceptibility starts to increase, probably because of thermally induced chemical alteration of clay or iron sulphide minerals.

The decrease in IRM at 330–360°C is characteristic of magnetic iron sulphide minerals such as pyrrhotite or greigite. Pyrrhotite does not undergo alteration upon heating, whereas greigite irreversibly breaks down (Dekkers, 1989; Roberts, 1995). Decreases in susceptibility are commonly observed during the breakdown of greigite (Roberts, 1995). This evidence suggests that greigite is more likely to be present than pyrrhotite. In addition to greigite, it appears that magnetite is also present in samples above ~140 mbsf (Fig. 11a). The behaviour of some discrete samples during AF demagnetisation (Fig. 12b) provides additional support for the presence of a magnetic iron sulphide. For some samples (e.g., between 135 and 146 mbsf), AF demagnetisation above 50 mT was obscured by the simultaneous acquisition of a gyroremanent magnetisation (GRM) (Stephenson, 1980, 1981). Acquisition of a GRM suggests the presence of a single-domain material, and sedimentary greigite most commonly occurs with single-domain-like properties (Roberts, 1995). In conjunction with thermal unblocking between 330 and 360°C, acquisition of a GRM provides strong evidence for the presence of a magnetic iron sulphide such as greigite in sediments from Site 1166 (e.g., Snowball, 1997; Hu et al., 1998; Sagnotti and Winkler, 1999).

4.5. Palaeomagnetic behaviour – ODP Site 1166

Stable palaeomagnetic behaviour is evident in vector component diagrams for 50% of discrete samples analysed from Hole 1166A. ChRM directions generally tend toward the origin of the plots and MAD values are $<10°$ (Fig. 12). For the other 50% of the samples, reliable ChRM directions could not be determined due to the dominance of low-coercivity overprints or to noisy behaviour on demagnetisation.

4.6. Magnetic polarity zonation – ODP Site 1166

The ChRM inclinations for discrete samples and long-core measurements have a clear bimodal distribution that demonstrates the dominance of two stable polarity states (Fig. 6c). Steep normal and reversed polarity inclinations, which are indistinguishable from the expected GAD values for the site latitude, are dominant. In conjunction with evidence from vector component diagrams (Fig. 12), this indicates that demagnetisation has successfully removed any secondary components of magnetisation. ChRM directions from 30 discrete samples agree with the long-core measurements (Fig. 13), which enables identification of a clear polarity signal for most of the sediments recovered at Site 1166; however, core recovery was poor and the magnetostratigraphic data are of limited value. Magnetostratigraphic interpretations are presented in Section 5.

5. Discussion

5.1. Correlation with the GPTS – ODP Site 1165

The magnetostratigraphic interpretation for the upper 50 mbsf of Hole 1165B (Fig. 7a) is well constrained by diatom and radiolarian biostratigraphies (Tables 1 and 2; Bohaty and Whitehead, 2001, in preparation; Whalen and Lazarus, 2001, submitted; Whitehead and Bohaty, 2001). The inclination record for this interval, when compared with the GPTS of Cande and Kent (1995), is consistent with the presence of parts of the Pleistocene and Pliocene from the Brunhes Chron (C1n) down to the upper part of the Thvera Subchron (C3n.4n). The last occurrence (LO) of *Thalassiosira kolbei* (PD3) is identified at 13.25 mbsf; however, poor preservation and low diatom abundance characterise the interval above this level to 9.25 mbsf, where *T. kolbei* is absent. The LO of *T. kolbei*, therefore, is broadly constrained to the interval between 9.25 and 17.25 mbsf. This datum consistently occurs within the Olduvai Subchron (C2n) (Baldauf and Barron, 1991; Harwood and Maruyama, 1992), which suggests that the thick interval of normal polarity between 6.97

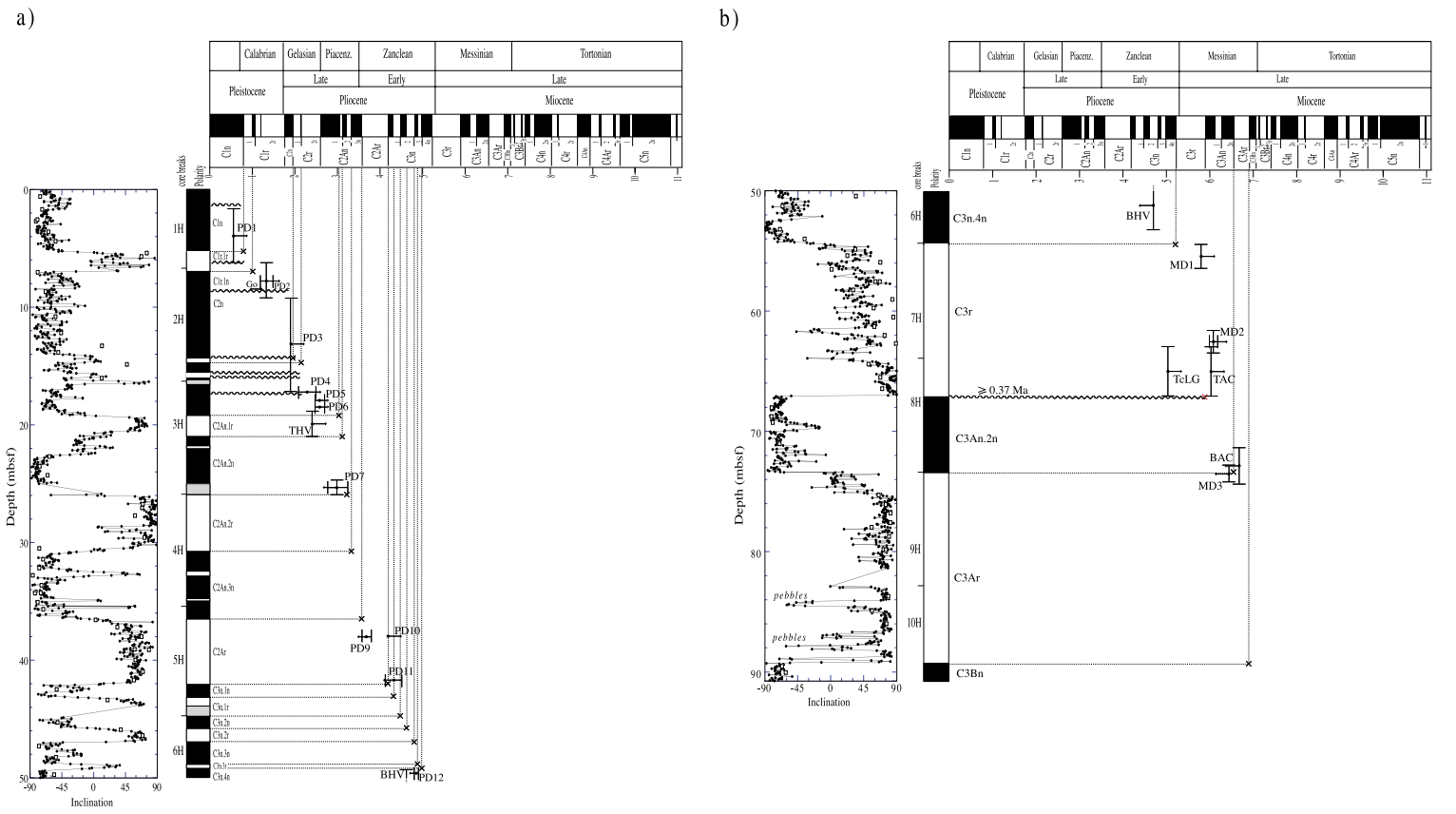

Fig. 7. Magnetostratigraphic record from Site 1165 for: (a) 0–50 mbsf, and (b) 50–91 mbsf. The palaeomagnetic inclination is shown after demagnetisation at 20–30 mT for the split cores (solid line) along with ChRM data for stepwise-demagnetised discrete samples (open squares). Polarity is shown on the log to the right. Black (white) = normal (reversed) polarity. Marine diatom (PD, MD) and radiolarian datums (Table 1; Whalen and Lazarus, 2001, submitted) are used to constrain the interpretation. The GPTS is from Cande and Kent (1995).

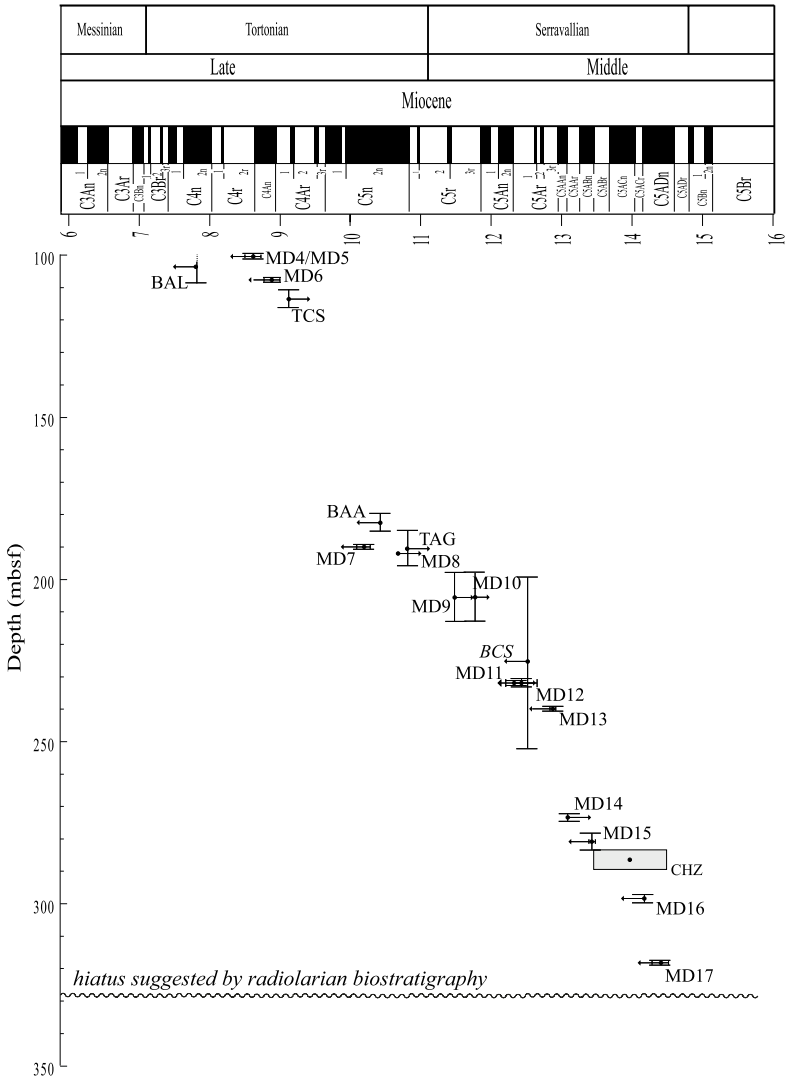

Fig. 8. Age interpretation for the interval from 100 to 350 mbsf for Site 1165. The polarity record is unresolved in this interval, therefore age interpretations rely solely on diatom (MD) and radiolarian datums, respectively, which indicate ages between about 8.5 and 14.5 Ma (Table 1; Whalen and Lazarus, 2001, submitted).

and 14.10 mbsf represents at least a portion of the Olduvai Subchron. The first occurrence (FO) of the calcareous nannofossil *Gephyrocapsa omega* (Go) at 8.46 mbsf (Fontanesi and Villa, in press) constrains the upper part of this normal polarity interval to the Jaramillo Subchron, which suggests a hiatus near 8.5 mbsf (≥ 0.70 Ma). The Pliocene–Pleistocene boundary occurs just above the Olduvai Subchron (Berggren et al., 1995). Thus, at Site 1165, the Pliocene–Pleistocene boundary should lie within the hiatus at 8.5 mbsf. Correlation with the GPTS is hampered by the presence of intervals with no recovery at core breaks, as indicated by sharp shifts in inclination (i.e., 6.97, 16.3 and 25.80 mbsf). In addition, significant disconformities must be present to explain the thinness of the Matuyama (C1r) and Brunhes (C1n) chrons. Based on our correlation with the GPTS,

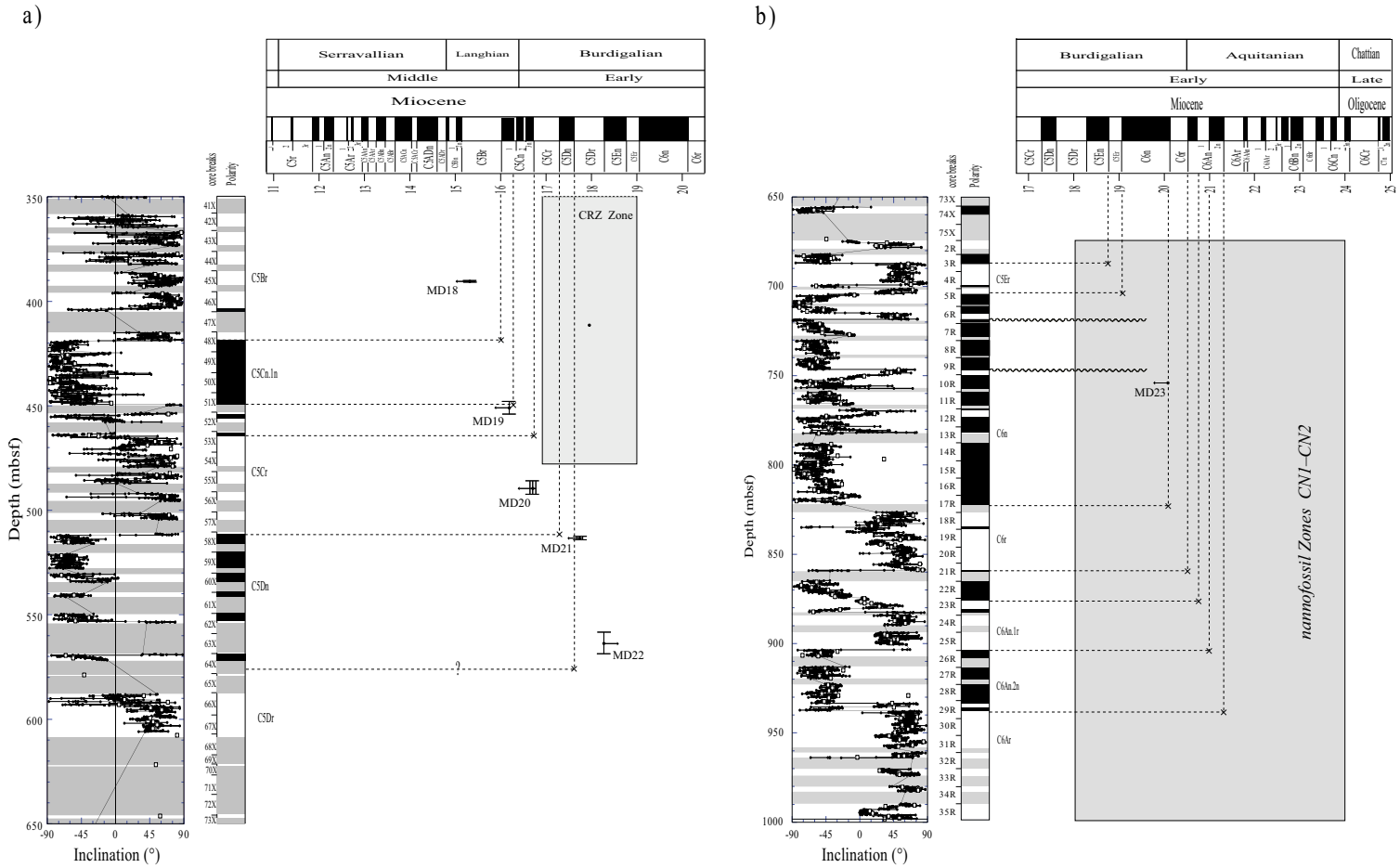

Fig. 9. Magnetostratigraphic record from Site 1165 for: (a) 350–650 mbsf, and (b) 650–999 mbsf. The palaeomagnetic inclination is shown after demagnetisation at 20–30 mT for the split cores (solid line) along with ChRM data for stepwise-demagnetised discrete samples (open squares). Polarity is shown on the log to the right. Black (white) = normal (reversed) polarity and shading indicates intervals with no core recovery. Marine diatoms (MD) (see Table 1) and sporadic calcareous nannofossil datums (zones CN1 and CN2) are used to constrain the interpretation. The GPTS is from Cande and Kent (1995).

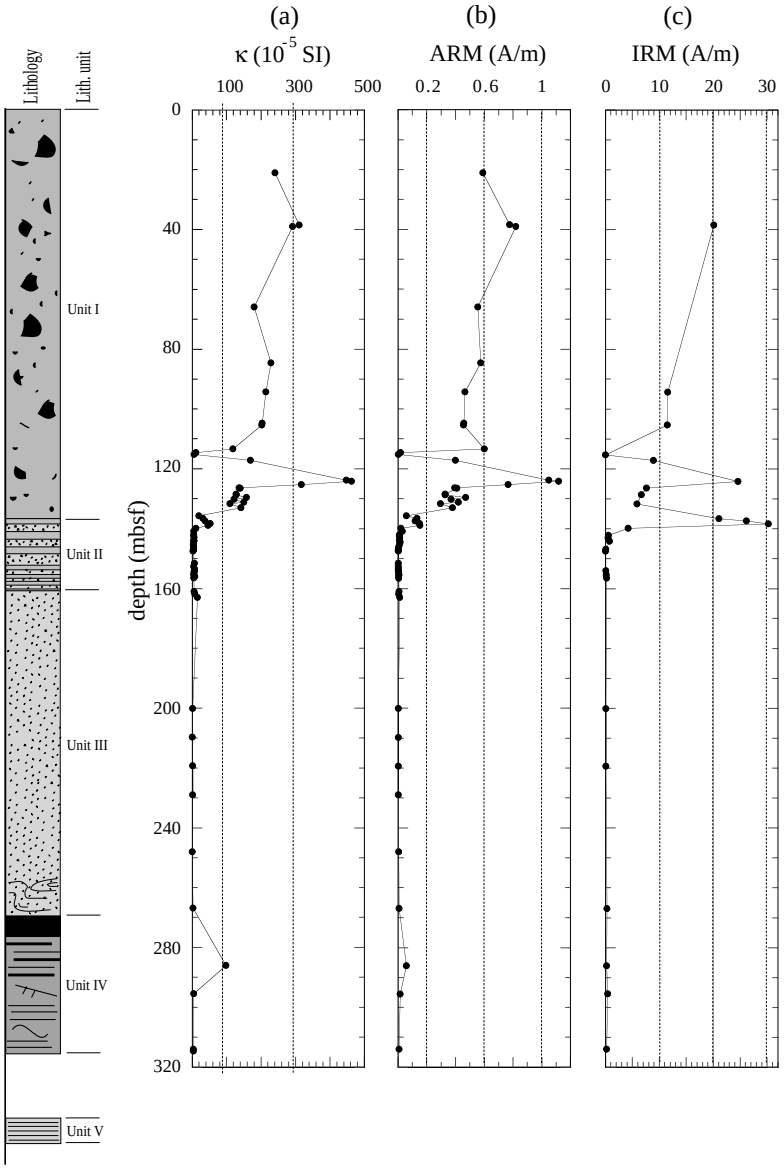

Fig. 10. Lithostratigraphic column and down-core variations of κ, ARM and IRM for Site 1166.

we suggest that disconformities must be present near 6.1, 14.3, 15.6, and ~16 mbsf. Correlation of the polarity zonation with the GPTS from the Olduvai Subchron down to 50 mbsf is reasonably well constrained by diatom datums. The absence of the diatom *Thalassiosira vulnifica* Zone and the *Thalassiosira insigna–T. vulnifica* Subzone 'b' of Harwood and Maruyama (1992) suggests that there is a disconformity at ~17.5 mbsf of 0.5–0.6 m.y. duration. The age interpretation for the upper 50 mbsf at Site 1165 implies a minimum sediment accumulation rate on the order of 10 m/m.y.

Proceeding down-core, the magnetic polarity zonation from 50 to about 91 mbsf is constrained by only a few biostratigraphic datums (Fig. 7b), which makes correlation with the GPTS more difficult. Starting from the upper part and following

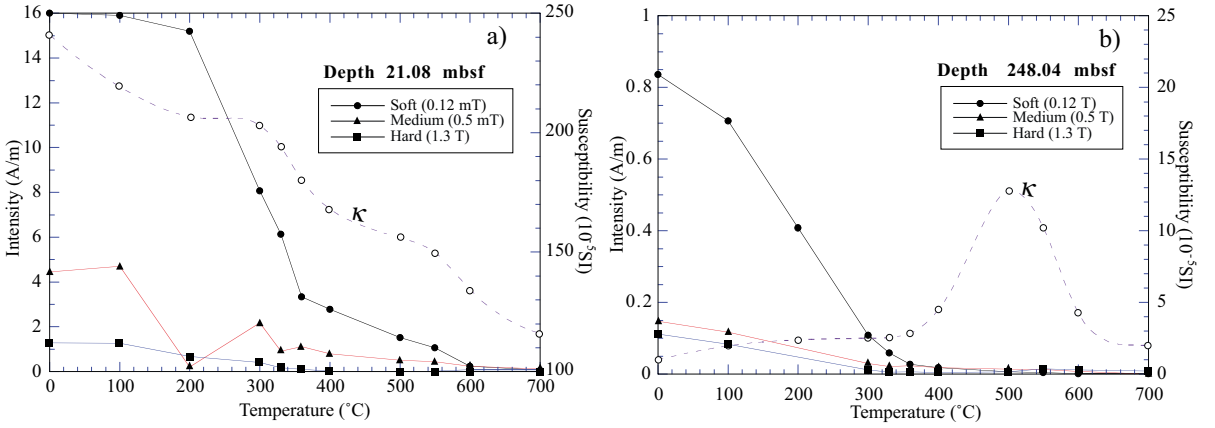

Fig. 11. Stepwise thermal demagnetisation of a composite three-axis IRM (see Lowrie, 1990) for two representative samples from 21.08 mbsf (Lithostratigraphic Unit I) and 248.04 mbsf (Lithostratigraphic Unit III) for Site 1166.

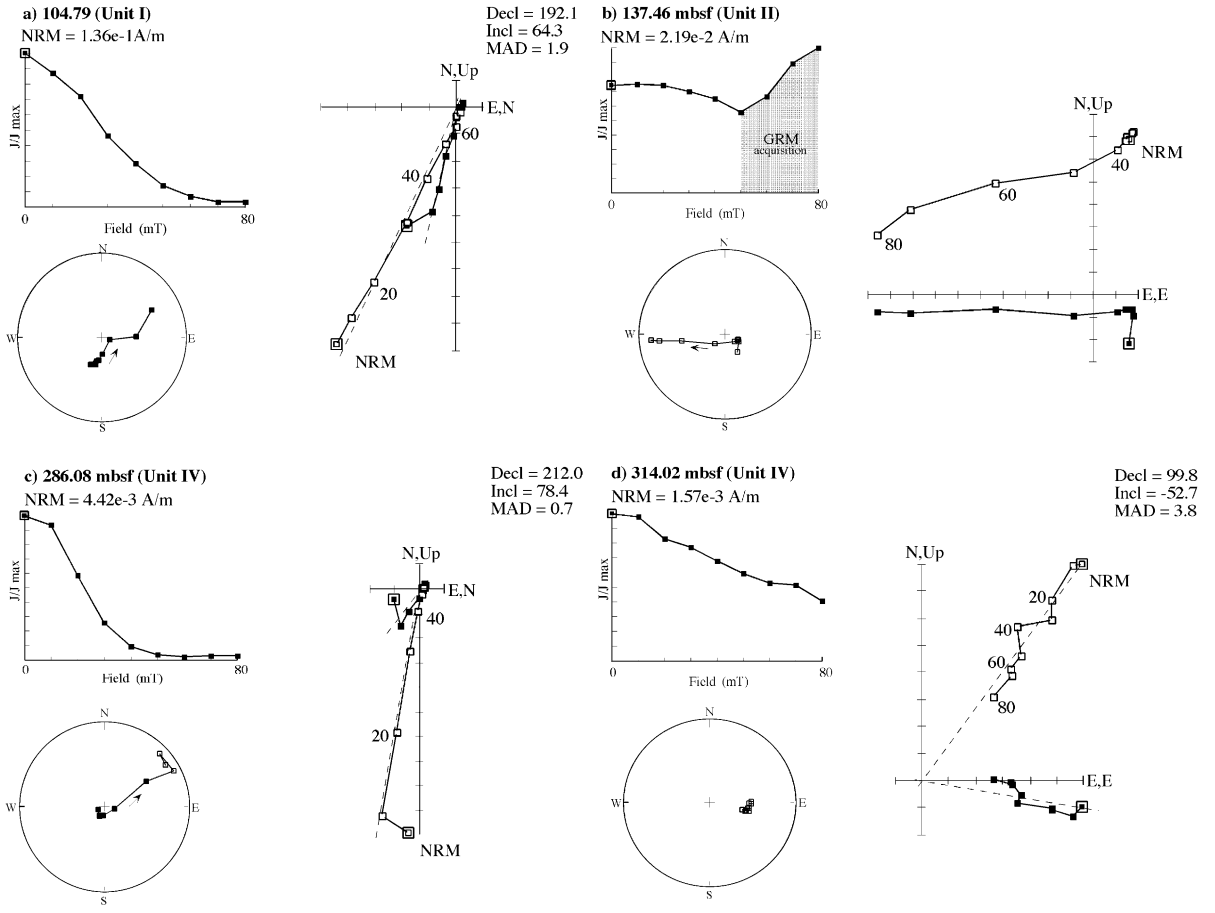

Fig. 12. AF demagnetisation behaviour for four representative samples from Site 1166. Conventions for the plots are the same as in Fig. 5. See text for description of results.

Table 1
Summary of Miocene–Pleistocene diatom datums recognised in ODP holes 1165B/C

Designation	Datum	Diatom taxon	Sample present	Level present (mbsf)	Sample absent	Level absent (mbsf)	Average depth (mbsf)	± (m)	Age (Ma)	Source(s)
Plio–Pleistocene										
PD1	LCO	*Actinocyclus ingens*	1165B-1H-5, 20–21	6.20	1165B-1H-2, 20–21	1.70	3.95	2.25	0.6–0.7	BB, HM, ZG
PD2	LO	*Fragilariopsis barronii*	1165B-2H-2, 95–96	9.25	1165B-1H-5, 20–21	6.20	7.73	1.53	1.2–1.5	BB, HM, GB, ZG
PD3	LO	*Thalassiosira kolbei*	1165B-3H-1, 95–96	17.25	1165B-2H-2, 95–96	9.25	13.25	4.00	1.8–2.0	BB, HM, ZG
PD4	LO	*Thalassiosira vulnifica*	1165B-3H-1, 127–129.5	17.57	1165B-3H-1, 117–120	17.47	17.52	0.05	2.1–2.5	ZG, WI
PD5	LO	*Thalassiosira insigna*	1165B-3H-2, 17–20	17.97	1165B-3H-2, 6–8.5	17.86	17.92	0.05	2.5–2.7	WI
PD6	LO	*Fragilariopsis weaveri*	1165B-3H-2, 67–70	18.47	1165B-3H-2, 57–59	18.37	18.42	0.05	2.5–2.7	ZG
PD7	FO	*Thalassiosira vulnifica*	1165B-3H-CC	25.01	1165B-4H-1, 20–21	26.00	25.51	0.49	2.7–3.2	BB, HM, WI
PD9	FO	*Fragilariopsis interfrigidaria*	1165B-5H-2, 117–119.5	37.97	1165B-5H-2, 125–126	38.05	38.01	0.04	3.7–3.8	BB, HM, WI, ZG
PD10	LO	*Rhizosolenia costata*	1165B-5H-2, 127–129.5	38.07	1165B-5H-2, 117–119.5	37.97	38.02	0.05	4.2	BB, HM
PD11	FO	*Fragilariopsis barronii*	1165B-5H-5, 47–50	41.77	1165B-5H-5, 60–61	41.90	41.84	0.06	4.2–4.3	BB, WI
PD12	FO	*Thalassiosira inura*	1165B-6H-4, 27–30	49.57	1165B-6H-4, 37–40	49.67	49.62	0.05	4.8–5.0	BB, CG
Miocene										
MD1	LO	*Nitzschia donahuensis*	1165C-1R-2, 95–96	56.45	1165C-1R-1, 59–60	54.59	55.52	0.93	5.8	HM
MD2	LO	*Nitzschia miocenica*	1165C-1R-7, 59–60	63.59	1165C-1R-6, 20–21	61.70	62.65	0.95	6.0–6.2	B, BB, BI
MD3	FO	*Thalassiosira miocenica*	1165B-8H-7, 20–21	73.00	1165B-9H-1, 95–96	74.25	73.63	0.63	6.4	BB, HM
MD4	FO	*Actinocyclus ingens* var. *ovalis*	1165B-11H-6, 20–21	99.43	1165B-12H-CC	101.80	100.62	1.18	8.5–8.7	G, HM, CG
MD5	FO	*Thalassiosira oliverana* var. *sparsa*	1165B-11H-6, 20–21	99.43	1165B-12H-CC	101.80	100.62	1.18	8.7	G, HM
MD6	FO	*Thalassiosira torokina*	1165B-13H-1, 20–21	106.50	1165B-13H-2, 20–21	108.00	107.25	0.75	8.8–9.0	HM/WI
MD7	FO	*Asteromphalus kennettii*	1165B-23X-3, 20–21	188.30	1165B-23X-4, 20–21	189.80	189.05	0.75	10.1–10.3	G, BB, CG
MD8	LCO	*Denticulopsis dimorpha* var. *areolata*	1165B-23X-6, 20–21	192.80	1165B-23X-5, 95–96	192.05	192.43	0.38	10.7	HM
MD9	LO	*Dent. praedimorpha* var. *minor/praedimorpha*	1165B-26X-CC	213.90	1165B-24X-3, 95–96	198.65	206.28	7.63	11.5	BB, HM
MD10	LO	*Nitzschia denticuloides*	1165B-26X-CC	213.90	1165B-24X-3, 95–96	198.65	206.28	7.63	11.7–11.9	HM, CG
MD11	FO	*Denticulopsis dimorpha* var. *areolata*	1165B-27X-6, 20–21	231.20	1165B-28X-1, 95–96	234.05	232.63	1.43	12.2–12.7	BB, HM, CG
MD12	LCO	*Crucidenticula nicobarica*	1165B-28X-1, 95–96	234.05	1165B-27X-6, 20–21	231.20	232.63	1.43	12.3	BB, HM
MD13	FO	*Dent. praedimorpha* var. *minor/praedimorpha*	1165B-28X-5, 20–21	239.30	1165B-28X-6, 20–21	240.80	240.05	0.75	12.8–12.9	G, CG
MD14	LO	*Denticulopsis hyalina*	1165B-33X-2, 95–96	274.05	1165B-33X-1, 20–21	271.80	272.93	1.13	13.1	YA
MD15	FCO	*Nitzschia denticuloides*	1165B-33X-7, 20–21	280.80	1165B-34X-1, 20–21	281.40	281.10	0.30	13.4–13.5	G, CG
MD16	FO	*Denticulopsis simonsenii*	1165B-35X-5, 95–96	297.45	1165B-36X-1, 20–21	300.00	298.73	1.27	14.2	G, BB, HM, CG
MD17	FO	*Actinocyclus ingens* var. *nodus*	1165B-37X-7, 20–21	318.30	1165B-38X-1, 95–96	319.65	318.98	0.67	14.3–14.5	HM, CG
MD18	FO	*Nitzschia grossepunctata*	1165B-45X-3, 95–96	390.05	1165B-45X-4, 20–21	390.80	390.43	0.38	15.2–15.4	HM, CG
MD19	FCO	*Actinocyclus ingens* s.s.	1165B-51X-4, 95–96	449.25	1165B-52X-1, 95–96	454.35	451.80	2.55	16.2	BB, HM
MD20	FO	*Denticulopsis maccollumii*	1165B-55X-4, 20–21	487.00	1165B-56X-1, 95–96	492.75	489.88	2.88	16.7–16.8	HM, CG
MD21	FO	*Crucidenticula ikebei*	1165B-58X-2, 20–21	512.70	1165B-58X-3, 95–96	514.95	513.83	1.13	17.7–18.0	HM
MD22	LCO	*Thalassiosira praefraga*	1165B-64X-1, 95–96	569.75	1165B-63X-CC	559.47	564.61	5.14	18.3	HM
MD23	FO	*Thalassiosira praefraga*	1165C-10R-3, 127–129	753.77	(*preservation*)	–	753.77	–	< 20.3–20.8	HM, YA
MD24	LO	*Rocella gelida*	(*absence*)	–	1165C-10R-3, 127–129	753.77	753.77	–	< 22.3	BB, HM

All diatom ages are calibrated to the Berggren et al. (1995) time scale and are compiled from the following sources: B = Baldauf (1985), G = Gersonde and Burckle (1990), BB = Baldauf and Barron (1991), HM = Harwood and Maruyama (1992), BI = Baldauf and Iwai (1995), GB = Gersonde and Bárcena (1998), YA = Yanagisawa and Akiba (1998), WI = Winter and Iwai (2002) and CG = Censarek and Gersonde (2002). Biostratigraphic datums are abbreviated as follows: LO = last occurrence datum, LCO = last common occurrence datum, FO = first occurrence datum, and FCO = first common occurrence datum.

Table 2
Summary of radiolarian datums recognised in ODP Hole 1165B

Designation	Datum	Radiolarian taxon	Top depth (mbsf)	Bottom depth (mbsf)	Average depth (mbsf)	± (m)	Young age (Ma)	Old age (Ma)
THV	LO	*Helotholus vema*	18.74	20.99	19.87	1.13	2.42	
BHV	FO	*Helotholus vema*	49.49	53.24	51.37	1.88	4.69	
TcLG	LCO	*Lychnocanoma grande*	63.19	66.99	65.09	1.94	5.02	
TAC	LO	*Amphymenium challengerae*	63.19	66.99	65.45	2.26	6.10	
BAC	FO	*Amphymenium challengerae*	71.49	74.24	72.87	1.38	6.65	
BAL	FO	*Acrosphaera labrata*	98.44	107.99	103.22	4.78	7.80	
TCS	LO	*Cycladophora spongothorax*	110.99	117.49	114.45	3.46	9.12	
BAA	FO	*Acrosphaera australis*	179.44	184.69	182.07	2.63	10.37	
TAG	LO	*Actinomma golownini*	184.69	196.39	190.54	5.85	10.77	
BCS	FO	*Cycladophora spongothorax*	198.64	252.59	225.62	26.98	12.55	
CHZ	Zone	*Cycladophora humerus* Zone	283.64	289.64			13.46	14.17
CRZ	Zone*approx	*Cycladophora golli regipileus*	346.74	478.79			16.90	19.00

the polarity pattern downward, the first two magnetozones can be correlated with the lower part of the Thvera Subchron (C3n.4n) and with Chron C3r. This interpretation seems reasonable based on available biostratigraphic constraints. The FO of *Thalassiosira miocenica* (MD3) at 73.63 ± 0.63 mbsf suggests that the normal–reverse–normal polarity sequence immediately beneath the sharp polarity transition at 67.02 mbsf correlates with chrons C3An.2n, C3Ar and C3Bn, respectively. Subchrons C3An.1n and C3An.1r are interpreted to be missing in a disconformity at the sharp polarity transition recorded at 67.02 mbsf. This interpretation suggests that a significant amount of time is missing at 67.02 mbsf (≥ 0.37 Ma). In this interpretation, the Miocene–Pliocene boundary, which lies below Chron C3n.4n on the polarity time scale (Berggren et al., 1995), is placed at ~ 55 mbsf in the uppermost part of a thick reversed polarity interval. Our age model for the interval between 50 and about 91 mbsf suggests a minimum sediment accumulation rate on the order of 20 m/m.y.

Relatively thin spikes in the inclination record, which are visibly related to the presence of igneous or metamorphic clasts, occur at 78.0 to 79.37 mbsf. Changes in polarity that occur at core breaks (e.g., 54.3 and 73.3 mbsf) probably indicate that time is missing at these depths.

Below 90 mbsf to about 350 mbsf (Fig. 8), the polarity record is unresolved because of unstable and weak magnetisations. Geochemical analyses indicate the presence of a broad peak in porewater silica concentration in this interval that is most likely derived from dissolution of biogenic silica (O'Brien et al., 2001). The depletion of magnetic minerals in this interval is higher than can be attributed solely to dilution by magnetite-poor sediments (such as biogenic silica), which implies that magnetite dissolution has occurred. Magnetite dissolution is commonly reported in areas with elevated organic carbon contents (Karlin and Levi, 1983; Canfield and Berner, 1987). Diatoms provide a significant source of organic carbon to the sea floor and it is likely that magnetite dissolution has occurred in conjunction with degradation of organic matter during early burial. However, thermodynamic calculations also indicate that magnetite is unstable under conditions with elevated dissolved silica concentrations (and appropriate Eh–pH conditions) and suggest that magnetite breaks down to produce iron-bearing smectite (Florindo et al., in press). It therefore seems likely that two mechanisms (i.e., reactions involving degradation of organic carbon and those involving dissolved silica) have operated to destroy the primary magnetic signal in this interval of Hole 1165B. Age interpretations for this depth interval therefore rely primarily on diatom and radiolarian biostratigraphies, which indicate a downward progression in age between about 8.5 and 14.5 Ma for the interval from 100 to 320 mbsf

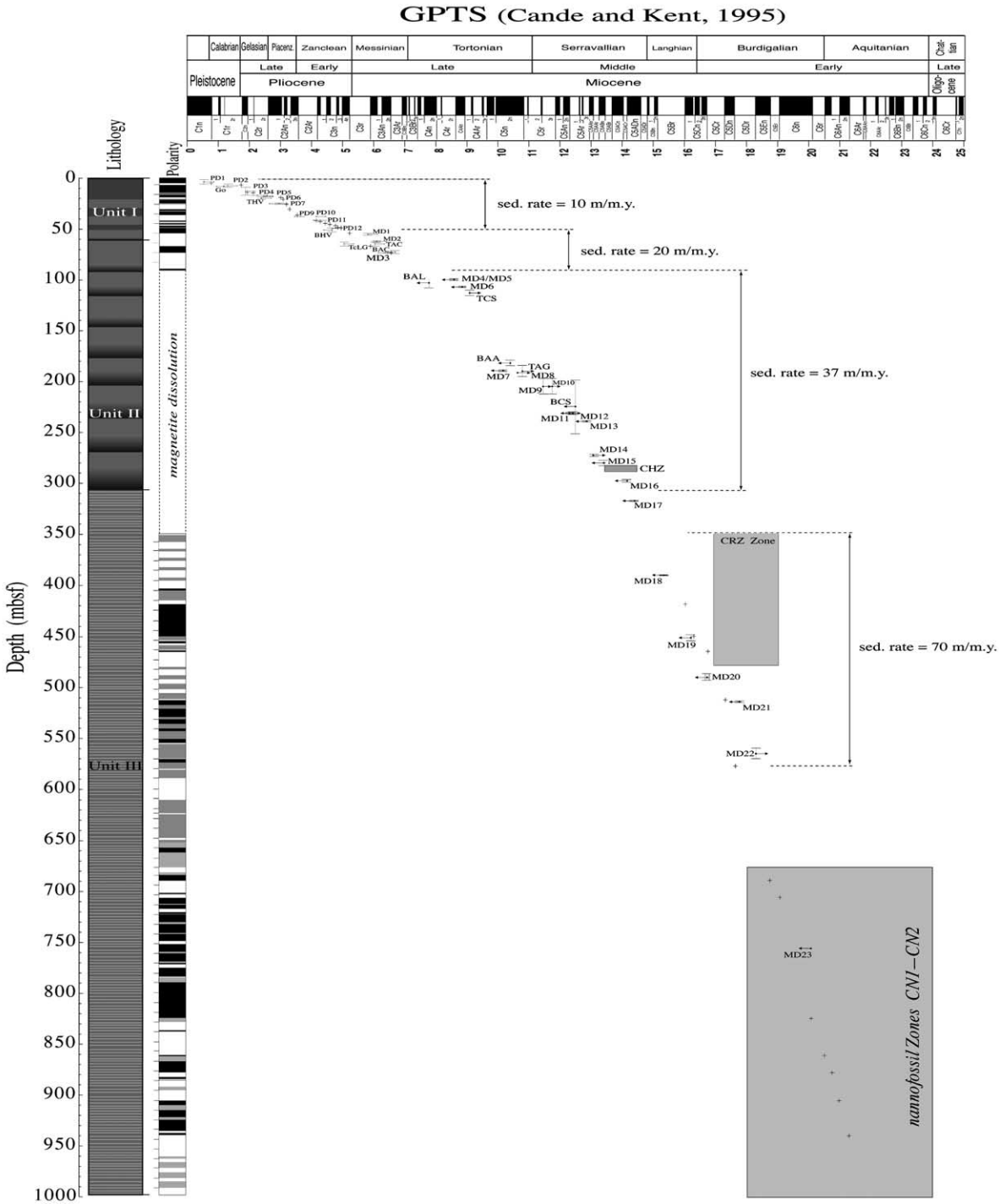

Fig. 14. Lithostratigraphic column and age–depth plot for ODP Site 1165. Biostratigraphic datums identified at Site 1165 are listed in Table 1.

(Tables 1 and 2; Bohaty and Whitehead, 2001, in preparation; Whalen and Lazarus, 2001, submitted; Whitehead and Bohaty, 2001). These constraints indicate a minimum sediment accumulation rate on the order of 37 m/m.y. A prominent lithological transition occurs at ~308 mbsf, from the dark-grey fissile claystones of Lithostratigraphic Unit III to the greenish-grey diatom-bearing clay of Lithostratigraphic Unit II. This transition is bounded by the FO of *Actinocyclus ingens* var. *nodus* (MD17) at 318.98 ± 0.67 mbsf and the FO of *Denticulopsis simonsenii* (MD16) at 298.73 ± 1.27 mbsf. Together, these datums indicate an age of ~14.3 Ma (within Chron C5ADn) for this level. Diatom biostratigraphy also indicates a possible hiatus at ~190–200 mbsf. The presence of a hiatus at this level, however, is not supported by radiolarian biostratigraphy.

Within Rock Magnetic Interval III (i.e., below about 350 mbsf), the sediments have more stable magnetisations and it is possible to obtain a magnetic polarity signal. The interval between ~350.0 and ~419.0 mbsf (Fig. 9a) is dominated by reversed polarity and is underlain by a normal polarity interval down to 449.4 mbsf. The FO of *Nitzschia grossepunctata* (MD18) at 390.43 ± 0.38 mbsf and the first common occurrence of *Actinocyclus ingens* s.s. (MD19) at 451.80 ± 2.55 mbsf tightly constrains these two magnetozones to correlate with chrons C5Br and C5Cn, respectively. The early–middle Miocene boundary is recognised within Chron C5Cn.2n, which is likely to occur at ~455–460 mbsf at Site 1165 (within Core 1165B-52X). Below the early–middle Miocene boundary, the FO of *Denticulopsis maccollumii* (MD20) at 489.88 ± 2.88 mbsf suggests that at least the upper part of the reversed polarity interval between about 463 and 512 mbsf might correlate with Chron C5Cr.

The FO of *Crucidenticula ikebei* (MD21) and the last common occurrence (LCO) of *Thalassiosira praefraga* (MD22) have been identified below 500 mbsf. These diatom datums suggest that the normal polarity magnetozone between 512 and about 575 mbsf (the base was not recovered) corresponds to Chron C5Dn and that the underlying reversed polarity interval corresponds to a portion of Chron C5Dr. This interpretation necessitates a younger age for the LCO of *Thalassiosira praefraga* than suggested by Harwood and Maruyama (1992). An older age interpretation for this level of the drillcore is possible, but it would require even greater conflict with the interpretation of the FO of *T. praefraga* (MD23). For the stratigraphic interval between 350 and about 575 mbsf, assuming that the top of Chron C5Br occurs at 350 mbsf, the presented chronostratigraphic constraints imply a minimum sediment accumulation rate on the order of 70 m/m.y.

The lowest occurrence of diatoms at Site 1165 is at ~754 mbsf (Fig. 9b). At this level, poorly preserved diatoms were observed in a sample from a carbonate-cemented burrow. *Thalassiosira praefraga* (MD23) is present within this assemblage, which places the interval between 492 and ~754 mbsf within the lower Miocene *T. praefraga* a–b subzones. This FO lies above a thick interval of poor diatom preservation, therefore, the presence of this taxon only provides a maximum age of 20.3–20.8 Ma for this level. Below about 754 mbsf, biogenic opal disappears because of the opal-A/opal-CT diagenetic transition and age assignments for the lower interval of Hole 1165C (754–999.1 mbsf) are inferred from sporadic calcareous nannofossils. A robust biostratigraphy could not be achieved, but the recovered assemblages indicate an early Miocene age, most likely encompassing nannofossil zones CN2 to CN1 (O'Brien et al., 2001). The polarity pattern recorded from 650 mbsf to the bottom of the core is tentatively correlated to the middle early Miocene portion of the GPTS (Fig. 9b), with a minimum age within Chron C6Ar (21.32–21.77 Ma) for the basal part of the recovered sequence. The presence of sharp changes in magnetic polarity (e.g., 718.4 and 746.4 mbsf) suggests the presence of more than one disconformity with significant missing time. The presence of possible disconformities in this part of the drillcore makes any correlation to the GPTS extremely difficult.

5.2. Antarctic glacial history as recorded at ODP Site 1165

Site 1165 was selected to intersect the base of a

thick sedimentary drift section, with the aim of dating the onset of drift formation and recording changes in sedimentation controlled by bottom currents and continental sediment supply. With the exception of the interval from about 90 to 350 mbsf, in which no palaeomagnetic interpretation was attempted and where the age interpretation relies primarily on diatom and radiolarian biostratigraphies, magnetisations in the remaining part of the core are stable. It is therefore possible to develop a reasonably constrained magnetobiostratigraphic chronology for Site 1165.

Site 1165 records a history of sedimentation on the continental rise extending back to earliest Miocene time (about 22 Ma). Several long-term changes characterise this record, including an overall trend of decreasing sedimentation rates from the bottom to the top of the hole (Fig. 14). There is a progressive decrease above about 308 mbsf, which is marked by a transition from the dark-grey fissile claystones of Lithostratigraphic Unit III (~999 to 308 mbsf) to the greenish-grey diatom-bearing clay of Lithostratigraphic Unit II (~308 to 64 mbsf). At the Unit III/II transition, ice-rafted debris, sand grains, and the total clay content also increase (O'Brien et al., 2001). The chronology presented above indicates a middle Miocene age (~14.3 Ma) for this lithological transition at Site 1165. Correlation to ODP Hole 747A (Schlich et al., 1989; Wise et al., 1992) on the Kerguelen Plateau supports this age assignment and suggests that the transition occurred within Chron C5ADn (Fig. 15). This correlation also suggests that the lithological transition observed in Hole 1165B is coincident with the base of the Mi-3/3a oxygen isotope event, which suggests a palaeoenvironmental control on middle Miocene sedimentation changes at Site

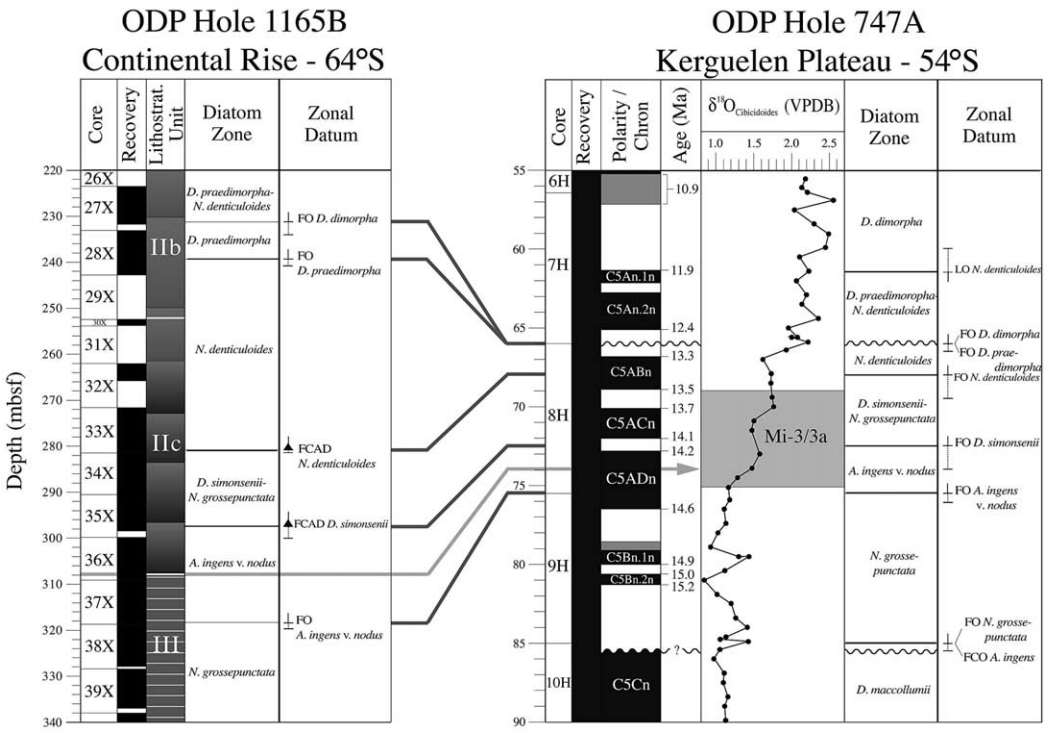

Fig. 15. Correlation between middle Miocene intervals of ODP holes 1165B (this study) and 747A (Kerguelen Plateau) based on diatom biostratigraphy. Data from Hole 747A are compiled from Harwood and Maruyama (1992), Harwood et al. (1992), Heider et al. (1992), Wright and Miller (1992), and Ramsay and Baldauf (1999). The mid-Miocene glacial event (Mi-3/3a) follows the nomenclature assigned by Miller et al. (1991).

Table 3
Summary of Plio–Pleistocene and Eocene diatom datums identified in ODP Hole 1166A

Designation	Datum	Diatom taxon	Sample present	Level present (mbsf)	Sample absent	Level absent (mbsf)	Age (Ma)	Source(s) (s)
Plio–Pleistocene								
PD1	LCO	*Actinocyclus ingens*	1R-CC	3.02	1R-2, 72–73	2.22	0.6–0.7	BB, HM, ZG
PD3	LO	*Thalassiosira kolbei*	13R-1, 65–66	113.95	(*preservation*)	–	> 1.8–2.0	BB, HM, ZG
PD4	LO	*Thalassiosira vulnifica*	13R-1, 123–124	114.53	13R-1, 80–83	114.10	2.1–2.5	ZG, WI
PD5	LO	*Thalassiosira insigna*	13R-1, 124–126	114.54	13R-1, 80–83	114.10	2.5–2.7	WI
PD7	FO	*Thalassiosira vulnifica*	13R-2, 65–67	115.45	(*preservation*)	117.25	< 2.7–3.2	BB, HM, WI
PD8	FO	*Thalassiosira elliptipora*	13R-CC	117.25	(*preservation*)	–		BB, HM
Eocene								
ED1	FO	*Rhizosolenia oligocaenica*	(*absence*)	–	–	–	> 33.7	BB, HM
ED2	LO	*Hemiaulus caracteristicus*	15R-3, 18–19	135.73	(*preservation*)	–	> 33	BB
ED3	LCO	*Distephanosira architecturalis*	15R-3, 18–19	135.73	(*preservation*)	–	> 33	GoC
ED4	LO	*Trinacria cormuta*	(*absence*)	–	17R-2, 58–59	153.48	< 37–42	Go, GoC

All diatom ages are calibrated to the Berggren et al. (1995) time scale and are compiled from the following sources: Go = Gombos (1983), GoC = Gombos and Cielsielski (1983), BB = Baldauf and Barron (1991), HM = Harwood and Maruyama (1992), WI = Winter and Iwai (2002), and ZG = Zielinski and Gersonde (in press). Biostratigraphic datums are abbreviated as follows: LO = last occurrence datum, LCO = last common occurrence datum, and FO = first occurrence datum.

1165. Recently, Mg/Ca ratios of benthic foraminifera have been used to estimate seawater palaeotemperatures and to separate the global ice-volume signal from oxygen isotopes. Using this technique, three periods of major ice sheet expansion have been identified. A large accumulation of ice in the middle Miocene has been associated with EAIS growth; ~85% of the benthic $\delta^{18}O$ increase at this time is attributed to an increase in continental ice volume (Lear et al., 2000; Billups and Schrag, 2002). The middle Miocene change in sedimentation at Site 1165 most likely reflects a change in a combination of factors, including local surface-water productivity, opal preservation, deep-water circulation/bottom currents, and the nature of terrigenous material shed from the continent and reworked from shelf areas. It might reflect an expansion of ice onto the continental shelf, with a progressive shift in the onshore sediment source area to palaeoenvironments that produced less terrigenous sedimentation, a lower-energy current regime, and more floating debris-charged icebergs at Site 1165.

5.3. Correlation to the GPTS – ODP Site 1166

In the stratigraphic interval from the sea floor down to 123 mbsf in Hole 1166A, magnetostratigraphic interpretation is difficult because of extremely poor core recovery and the low abundance of microfossils (Fig. 13). Diamictons in the upper part of the hole and sandy sediments in the lower part were both difficult to recover with ODP drilling technology. In addition to poor core recovery, fossil occurrences are sporadic throughout the core, and biostratigraphic age control is limited to narrow stratigraphic intervals (Table 3).

Reversed polarity is recorded in the uppermost sediment recovered in Hole 1166A, which indicates that the normal polarity Brunhes Chron was not recorded at this site. Although diatoms are poorly preserved in this interval, an abundant and well-preserved diatom assemblage occurs in a biosiliceous sponge-spicule horizon in sample 1166A-1R-2, 72–73 cm (2.22 mbsf). This assemblage consists entirely of extant Southern Ocean diatoms. The absence of the fossil diatom species

Actinocyclus ingens (LO 0.66 Ma, datum PD1) in this assemblage indicates that the interval above 2.22 mbsf is <0.66 Ma in age (O'Brien et al., 2001). These biostratigraphic data conflict with the observed polarity for the interval between 0.00 and 2.22 mbsf, which indicates a minimum age of 0.78 Ma (top of the Matuyama Chron). Sediments from Core 1166A-1R are moderately disturbed and it is unlikely that the uppermost part of the sediment record was recovered with rotary drilling. Also, the stable ChRM may have been produced by drilling disturbances, and it may not be primary. The palaeontological samples were taken from a distinct in situ sponge-spicule-rich bed and are unlikely to be contaminated.

Well-preserved marine diatoms of late Pliocene age are present within two greenish-grey silt horizons in Core 188-1166A-13R (113.30–117.25 mbsf) (O'Brien et al., 2001). Several diatom datums constrain the age of this interval, including the LO of *Thalassiosira kolbei* (PD3), the LO of *Thalassiosira vulnifica* (PD4), the LO of *Thalassiosira insigna* (PD5), the FO of *T. vulnifica* (PD7), and the FO of *Thalassiosira elliptipora* (PD8). These datums broadly place the age of this section between 2.0 and 3.0 Ma. We correlate the reversed–normal–reversed polarity pattern between 113.40 and 117.12 mbsf to the lower part of chrons C2r.1r, C2r.1n (Réunion) and to the upper part of Chron C2r.2r. This interpretation requires diachroneity in the LO of *T. insigna* (calibrated at 2.5–2.6 Ma by Baldauf and Barron (1991) and Harwood and Maruyama (1992)) between Site 1166 and more northerly sites on the Kerguelen Plateau. With this interpretation, the LO of *T. insigna* at Site 1166 would range above the top of Chron C2r.1n (2.14 Ma). A correlation to Chron C2An.1n (upper Gauss), however, cannot be completely ruled out by the diatom data. Our preferred correlation with Chron C2r.1n implies that Chron C2n (Olduvai Subchron) is missing in Hole 1166A. The reversed polarity interval recorded above $\sim$110 mbsf therefore probably provides a discontinuous record of the Matuyama Chron (C1r.2r and C1r.1r). Additionally, using the Southern Ocean diatom zonation of Harwood and Maruyama (1992), the absence of *T. vulnifica* in the 'upper' silt bed suggests that the 'upper' and 'lower' silt horizons in Core 188-166A-13R may be separated by a disconformity at 114.53–114.10 mbsf (O'Brien et al., 2001). In contrast, application of the Antarctic Shelf diatom zonation of Winter and Harwood (1997) suggests that the Pliocene beds are not separated by a disconformity. The presence of a disconformity can only be assessed with additional age information because reversed polarity is observed above and below this level. The recovered sections below Core 1166A-13R, from 123.14 to 135.41 mbsf, lack biostratigraphic constraints, which precludes correlation to the GPTS.

An abrupt unconformity occurs within core section 1166A-15R-2 at 135.41 mbsf between dark-grey diamictons (Lithostratigraphic Unit I) and olive-grey diatom-bearing claystones (Lithostratigraphic Unit II). Immediately beneath this lithological contact, palaeomagnetic inclinations have reversed polarity down to 136.32 mbsf, followed down-core by a thick interval of normal polarity (between 136.32 and $\sim$148.0 mbsf). Diatoms are present and are moderately diverse between 135.73 and 152.70 mbsf. The LO of *Hemiaulus caracteristicus* (ED2) and the LCO of *Distephanosira architecturalis* (ED3) at 135.73 mbsf provide a minimum age of $\sim$33 Ma for this part of the record. This raises the possibility that the reversed–normal polarity interval immediately below the unconformity may correlate with the lowermost part of Chron C12r and the upper part of Chron C13n, respectively. In this interpretation, the E–O boundary (33.7 Ma), which occurs in the upper part of Chron C13r (Berggren et al., 1995), would lie below the interval with normal polarity (i.e., below 160 mbsf) within the upper part of Lithostratigraphic Unit III. The diatom data, however, do not provide a well-constrained maximum age, and correlation to a normal polarity chron within chrons C15 through C17 is equally possible. The absence of *Rhizosolenia oligocaenica* (FO 33.7 Ma) further suggests that the interval of normal polarity between 136.32 and 148.0 mbsf may not correlate with Chron C13n.

From $\sim$153 mbsf to the bottom of Lithostratigraphic Unit III (267.17 mbsf), the sediments are barren of fossils, except for relatively abundant

palynomorphs which allow broad determination of a mid–late Eocene age for this interval (Truswell and Macphail, 2001). Spores, pollen and dinocysts are abundant in most sampled cores, and age control is primarily provided by the dinocysts, with reinforcement from a limited number of spore and pollen taxa.

All core-catcher samples below 267.17 mbsf yielded relatively sparse palynofloras that indicate a Late Cretaceous age. Dinoflagellate cysts in this lower interval of Hole 1166A are relatively rare, and a provisional age determination of Turonian–?Santonian rests largely on age diagnostic spores and gymnosperm pollen abundances (Truswell and Macphail, 2001). These constraints suggest that the three intervals of normal polarity recorded below 286 mbsf (Lithostratigraphic Unit IV) might represent the uppermost part of the Cretaceous normal superchron. In addition, the Turonian–?Santonian section recovered at Site 1166 may correlate to a similar section drilled at Site 742 during ODP Leg 119 (Barron et al., 1989, 1991).

5.4. *Antarctic glacial history as recorded at ODP Site 1166*

Growth of a large, continental-scale ice sheet on East Antarctica is believed to have initiated near the E–O boundary. However, to date, drilling on the continent and continental margin has not recovered a stratigraphic section that clearly spans and includes the transition from the so-called mid-Cretaceous 'greenhouse world' to the late Cenozoic 'icehouse world' (Shackleton and Kennett, 1975; Miller et al., 1987; Prothero, 1994). A primary objective of Leg 188 was achieved at Site 1166 by recovering a set of cores, albeit with poor recovery and significant disconformities, that penetrate below the glacial deposits sampled at Site 742 and that are interpreted as late middle Eocene to early Oligocene in age by Barron et al. (1991). It should be noted that this middle Eocene age determination for glacial strata should not be considered definitive since the reported middle Eocene calcareous nannofossil might have been reworked. Sites 742 and 1166 record brief intervals in the history of the EAIS for the Prydz Bay region, extending back through the early stage of glaciation to pre-glacial times. Pre-glacial to early glacial times are recorded by the Turonian fluvio-lacustrine and lagoonal deposits, which are unconformably overlain by sandy fluvio-deltaic units of mid–late Eocene age. These units are overlain by late Eocene to early Oligocene glacimarine deposits (Shipboard Scientific Party, 2001b). Pollen and spores indicate an Austral conifer woodland that grew in humid and mild-temperature conditions in the Late Cretaceous, with a change to cool temperate *Nothofagus* rainforest or scrub with subcanopy flora in the mid–late Eocene (Macphail and Truswell, submitted).

Correlation between ODP sites 1166 and 742, by comparison of down-hole logs and regional seismic stratigraphy, indicates that Lithostratigraphic Units I and II at Site 1166 are equivalent to (or older than) similar units at Site 742. Below the level of Unit II, however, samples from Site 1166 are stratigraphically lower and record a more temperate alluvial facies than at Site 742. The lower part of Lithostratigraphic Unit III (i.e., the deformed organic-rich sands and silts) may have been sampled in the lower 2 m of Site 742. If the organic units are the same, then the overlying thick section of sands (Lithostratigraphic Unit III) is missing at Site 742. The deepest unit at Site 1166 (Lithostratigraphic Unit V) lies below a regional seismic unconformity that can be traced to ODP Site 741 (68°23.16′S, 76°23.02′E), about 110 km away. Similar pre-glacial, Early Cretaceous grey claystone deposits, like those of Lithostratigraphic Unit V at Site 1166, were sampled at Site 741 (Barron et al., 1989).

6. Conclusions

The early stages of glaciation in East Antarctica (i.e., from the Eocene to the mid-Miocene) are recorded in the studied ODP cores recovered from Prydz Bay on Leg 188. We present results from the continental shelf and rise that document the Cretaceous–Palaeogene transition from pre-glacial conditions to glacial conditions on the shelf (Site 1166), and a long-term lower to upper

Miocene change in sedimentation that most likely reflects a change in the mode and scale of EAIS glaciation (Site 1165). The deepest cores recovered at Site 1166, although limited by poor recovery, provide evidence of pre-glacial times. A Turonian fluvio-lacustrine unit, lagoonal deposits and sandy fluvio-deltaic units of mid–late Eocene age contain a record of the transition from humid and mild conditions to cool temperate conditions. At this time, the Antarctic continent was still connected with South America and Australia and oceanic circulation was mainly meridional (Kennett, 1977). A seaway, which provided a pathway for deep circum-Antarctic oceanic circulation and which led to marked cooling on the continent (Kennett, 1977), did not open until the E–O boundary at 33.6 Ma, when dated sea floor magnetic anomalies and clear fracture zone lineations (Royer and Rollet, 1997; Marks et al., 1999) indicate that the South Tasman Rise cleared the Oates Land Coast of East Antarctica. This opening may have produced the large positive shift ($>1.0‰$) in the global Cenozoic oxygen isotope record ($\delta^{18}O$ event Oi-1; Miller et al., 1991). The Drake Passage, between the southern tip of South America and the northern end of the Antarctic Peninsula, then opened to deep-water circulation by 31 ± 2 Ma (Lawver et al., 1991, 1992; Lawver and Gahagan, 2001, 2003).

The major change in sedimentation recorded at Site 1165 (307.8 mbsf; ~14.3 Ma) marks a phase of renewed channel incision and a reduction in sediment wave formation on the Wild Drift flank (O'Brien et al., 2001). This transition could be associated with the second major phase of Antarctic ice sheet expansion, which occurred during the middle Miocene and which is expressed by a c. 0.6‰ positive shift (event Mi-3/3a) in benthic foraminiferal $\delta^{18}O$ values (Flower and Kennett, 1995; Lear et al., 2000; Zachos et al., 2001). This shift followed a warm phase that peaked in the early middle Miocene climatic optimum (17–15 Ma) (Zachos et al., 2001).

In order to further improve our understanding of Antarctic glacial history, more comparisons with sequences drilled elsewhere on the Antarctic margin are needed, in addition to more Antarctic continental-margin drilling transects. This will provide the proximal geological control needed to link the histories of the Antarctic ice sheets with global sea level, palaeoclimate and palaeoceanographic changes. To date, continental-margin drilling transects are still too few in number but future long-term drilling initiatives are in the planning stages (Cooper et al., 2002).

Acknowledgements

We are grateful to the ODP Leg 188 shipboard scientific party for their support and encouragement. Participation of F.F. and P.S.E. on Leg 188 was supported by the UK NERC. F.F. also gratefully acknowledges support from the Italian Programma Nazionale di Ricerche in Antartide and A.P.R. and F.F. acknowledge support from EU contract ERBFMRXCT98-0247 (MAG-NET). S.M.B. and J.M.W. gratefully acknowledge funding and support provided by JOI-USSAC. We wish to thank D. Lazarus for his valuable suggestions. This research used samples and data provided by the Ocean Drilling Program, which is sponsored by the U.S. National Science Foundation and participating countries under the management of Joint Oceanographic Institutions, Incorporated.

References

Anson, G.L., Kodama, K.P., 1987. Compaction-induced shallowing of the post-depositional remanent magnetization in a synthetic sediment. Geophys. J.R. Astron. Soc. 88, 673–692.

Arason, P., Levi, S., 1990. Compaction and inclination shallowing in deep sea sediments from the Pacific Ocean. J. Geophys. Res. 95, 4501–4510.

Baldauf, J.G., 1985. A high-resolution late Miocene-Pliocene diatom biostratigraphy for the eastern equatorial Pacific. In: Mayer, L., Theyer, F., Thomas, E. et al. (Eds.), Init. Rep. DSDP, Vol. 85. U.S. Govt. Printing Office, Washington, DC, pp. 457–475.

Baldauf, J.G., Barron, J.A., 1991. Diatom biostratigraphy: Kerguelen Plateau and Prydz Bay regions of the Southern Ocean. In: Barron, J., Larsen, B. et al. (Eds.), Proc. ODP, Sci. Res., Vol. 119. Ocean Drilling Program, College Station, TX, pp. 547–598.

Baldauf, J.G., Iwai, M., 1995. Neogene diatom biostratigraphy for the eastern equatorial Pacific Ocean, Leg 138. In: Pisias,

N.G., Mayer, L.A., Janecek, T.R., Palmer-Julson, A., van Andel, T.H. (Eds.), Proc. ODP, Sci. Res., Vol. 138. Ocean Drilling Program, College Station, TX, pp. 105–128.

Barr, S.R., Januszczak, N., Williams, T., Handwerger, D.A., 2001. Determining the glacial history of Prydz Bay, Antarctica: observations based on the integration of downhole logging data and sedimentological description, Leg 188, Hole 1166. In: Florindo, F., Cooper, A.K. (Eds.), The Geologic Record of the Antarctic Ice Sheet from Drilling, Coring and Seismic Studies, Extended Abstract Volume for the Int. ANTOSTRAT Symp. Quad. Geofis. 16, 11–12, 2001.

Barron, J., Larsen, B. et al., 1989. Proc. ODP Init. Rep., Vol. 119. Ocean Drilling Program, College Station, TX.

Barron, J., Larsen, B. et al., 1991. Proc. ODP, Sci. Res., Vol. 119. Ocean Drilling Program, College Station, TX.

Berggren, W.A., Kent, D.V., Swisher, III, C.C., Aubrey, M.P., 1995. A revised Cenozoic geochronology and biostratigraphy. In: Berggren, W.A., Kent, D.V., Aubrey, M.P., Hardenbol, J. (Eds.), Geochronology, Time Scales, and Stratigraphic Correlation. Soc. Econ. Paleontol. Mineral. Spec. Publ. 54, 129–212.

Billups, K., Schrag, D.P., 2002. Paleotemperatures and ice volume of the past 27 Myr revisited with paired Mg/Ca and $^{18}O/^{16}O$ measurements on benthic foraminifera. Paleoceanography 17(1), 1029/2000PA000567, 3-1 to 3-11.

Bohaty, S.M., Whitehead, J.M., Miocene diatom biostratigraphy of ODP site 1165, Antarctic continental rise, In: Florindo, F., Cooper, A.K. (Eds.), The Geologic Record of the Antarctic Ice Sheet from Drilling, Coring and Seismic Studies, Extended Abstract Volume for the Int. ANTOSTRAT Symp. Quad. Geofis. 16, 23–24.

Bohaty, S.M., Whitehead, J.M., Miocene diatom biostratigraphy of ODP Holes 1165B and 1165C, Antarctic continental rise. Micropaleontology, in preparation.

Cande, S.C., Kent, D.V., 1995. Revised calibration of the geomagnetic polarity time scale for the Late Cretaceous and Cenozoic. J. Geophys. Res. 100, 6093–6095.

Canfield, D.E., Berner, R.A., 1987. Dissolution and pyritization of magnetite in anoxic marine sediments. Geochim. Cosmochim. Acta 51, 645–659.

Censarek, B., Gersonde, R., 2002. Miocene diatom biostratigraphy at ODP Sites 689, 690, 1088, 1092 (Atlantic sector of the Southern Ocean). Mar. Micropal. 45, 309–356.

Chand, S., Radhakrishna, M., Subrahmanyam, C., 2001. India-East Antarctica conjugate margins: rift-shear tectonic setting inferred from gravity and bathymetry data. Earth Planet. Sci. Lett. 185, 225–236.

Cooper, A., Stagg, H., Geist, E., 1991. Seismic stratigraphy and structure of Prydz Bay, Antarctica: implications from Leg 119 drilling. In: Barron, J., Larsen, B. et al. (Eds.), Proc. ODP, Sci. Res., Vol. 119. Ocean Drilling Program, College Station, TX pp. 5–26.

Cooper, A.K., O'Brien, P.E., ODP Leg 188 Shipboard Scientific Party, 2001. Early stages of East Antarctic glaciation – insights from drilling and seismic reflection data in the Prydz Bay region. In: Florindo, F., Cooper, A.K. (Eds.), The Geologic Record of the Antarctic Ice Sheet from Drilling, Coring and Seismic Studies, Extended Abstract Volume for the Int. ANTOSTRAT Symp. Quad. Geofis. 16, 185–186.

Cooper, A.K., Barrett, P.J., Florindo, F., 2002. New inferences on Antarctic ice sheets and Cenozoic paleoclimates. EOS Trans. Am. Geophys. Union 83, 35–36.

Dekkers, M.J., 1989. Magnetic properties of natural pyrrhotite. II. High- and low-temperature behaviour of *Jrs* and TRM as function of grain size. Phys. Earth Planet. Inter. 57, 266–283.

Ehrmann, W.U., 1991. Implications of sediment composition on the southern Kerguelen Plateau for paleoclimate and depositional environment. In: Barron, J.A., Larsen, B. et al. (Eds.), Proc. ODP, Sci. Res., Vol. 119, Ocean Drilling Program, College Station, TX, pp. 185–210.

Fedorov, L.V., Grikurov, G.E., Kurinin, R.G., Masolov, V.N., 1982. Crustal structure of the Lambert Glacier area from geophysical data. In: Craddock, C. (Ed.), Antarctic Geoscience. Univ. Wisconsin Press, Madison, WI, pp. 931–936.

Florindo, F., Wilson, G.S., Roberts, A.P., Sagnotti, L., Verosub, K.L., 2001. Magnetostratigraphy of late Eocene–early Oligocene strata from the CRP-3 Core, McMurdo Sound, Ross Sea, Antarctica. Terra Ant. 8, 599–614.

Florindo, F., Roberts, A.P., Palmer, M., in press. Magnetite dissolution in siliceous sediments. Geochem. Geophys. Geosys.

Flower, B.P., Kennett, J.P., 1995. Middle Miocene deepwater paleoceanography in the southwest Pacific: relations with East Antarctic Ice Sheet development. Paleoceanography 10, 1095–1112.

Fontanesi, G., Villa, G., in press. Quaternary calcareous nannofossils from ODP leg 188 site 1165 (Prydz Bay, Antarctica). Proc. INA9, Int. Nannoplankton Assoc. Conf., 9–12 September 2002, University of Parma, Italy.

Fuller, M., Hastedt, M., Herr B., 1998. Coring-induced magnetization of recovered sediment. In: Weaver, P.P.E., Schmincke, H.-U., Firth, J.V., Duffield, W. (Eds.), Proc. ODP, Sci. Res., Vol. 157. Ocean Drilling Program, College Station, TX, pp. 47–56.

Gersonde, R., Bárcena, M.A., 1998. Revision of the upper Pliocene-Pleistocene diatom biostratigraphy for the northern belt of the Southern Ocean. Micropaleontology 44, 84–98.

Gersonde, R., Burckle, L.H., 1990. Neogene diatom biostratigraphy of ODP Leg 113, Weddell Sea (Antarctic Ocean). In: Barker, P.F., Kennett, J.P. et al. (Eds.), Proc. ODP, Sci. Res., Vol. 113. Ocean Drilling Program, College Station, TX, pp. 761–789.

Gombos, A.M., 1983. Middle Eocene diatoms from the South Atlantic. In: Ludwig, W.J., Krasheninikov, V.A. et al. (Eds.), Init. Rep. DSDP, Vol. 71. U.S. Govt. Printing Office, Washington, DC, pp. 565–581.

Gombos, A.M., Ciesielski, P.F., 1983. Late Eocene to early Miocene diatoms from the southwest Atlantic. In: Ludwig, W.J., Krasheninikov, V.A. et al. (Eds.), Init. Rep. DSDP, Vol. 71. U.S. Govt. Printing Office, Washington, DC, pp. 583–634.

Hambrey, M.J., Dowdeswell, J.A., 1994. Flow regime of the

Lambert Glacier-Amery Ice Shelf system, Antarctica: structural evidence from Landsat imagery. Ann. Glaciol. 20, 401–406.

Hambrey, M.J., McKelvey, B.C., 2000. Major Neogene fluctuations of the east Antarctic ice sheet: stratigraphic evidence from the Lambert Glacier region. Geology 28, 887–890.

Harwood, D.M., Maruyama, T., 1992. Middle Eocene to Pleistocene diatom biostratigraphy of Southern Ocean sediments from the Kerguelen Plataeu, Leg 120. In: Wise Jr., S.W., Schlich, R. et al. (Eds.), Proc. ODP, Sci. Res., Vol. 120. Ocean Drilling Program, College Station, TX, pp. 683–733.

Harwood, D.M., Webb, P.N., Barrett, P.J., 1992. The search for consistency between several indices of Antarctic Cenozoic glaciation. In: Cenozoic Glaciations and Deglaciations, Abstracts. Burlington House, London, pp. 61–63.

Heider, F., Leitner, B., Inokuchi, H., 1992. High southern latitude magnetostratigraphy and rock magnetic properties of sediments from sites 747, 749, and 751. In: Wise Jr., S.W., Schlich, R. et al. (Eds.), Proc. ODP, Sci. Res., Vol. 120. Ocean Drilling Program, College Station, TX, pp. 225–245.

Hrouda, F., 1994. A technique for the measurement of thermal changes of magnetic susceptibility of weakly magnetic rocks by the CS-2 apparatus and KLY-2 Kappabridge. Geophys. J. Int. 118, 604–612.

Hu, S., Appel, E., Hoffmann, V., Schmahl, W.W., Wang, S., 1998. Gyromagnetic remanence acquired by greigite (Fe_3S_4) during static three-axis alternating field demagnetization. Geophys. J. Int. 134, 831–842.

Huybrechts, P., 1993. Glaciological modelling of the late Cenozoic East Antarctic ice sheet: stability or dynamism? Geogr. Ann. 75A, 221–238.

Karlin, R., Levi, S., 1983. Diagenesis of magnetic minerals in Recent haemipelagic sediments. Nature 303, 327–330.

Kennett, J.P., 1977. Cenozoic evolution of Antarctic glaciation, the circum-Antarctic ocean, and their impact on global paleoceanography. J. Geophys. Res. 82, 3843–3860.

Kirschvink, J.L., 1980. The least-squares line and plane and the analysis of palaeomagnetic data. Geophys. J.R. Astron. Soc. 62, 699–718.

Lawver, L.A., Royer, J.Y., Sandwell, D.T., Scotese, C.R., 1991. Crustal development: Gondwana break-up. In: Thomson, M.R.A., Crame, J.A., Thomson, J.W. (Eds.), Geological Evolution of Antarctica. Cambridge Univ. Press, Cambridge, pp. 533–539.

Lawver, L.A., Gahagan, L.M., Coffin, M.F., 1992. The development of paleoseaways around Antarctica. In: Kennett, J.P., Warnke, D.A. (Eds.), The Antarctic Paleoenvironment: A Perspective on Global Change. Am. Geophys. Union Ant. Res. Ser. 56, 7–30.

Lawver, L.A., Gahagan, L.M., 2001. Cenozoic evolution of the Antarctic continental margin and opening of southern ocean seaways. In: Florindo, F., Cooper, A.K. (Eds.), The Geologic Record of the Antarctic Ice Sheet from Drilling, Coring and Seismic Studies, Extended Abstract Volume for the Int. ANTOSTRAT Symp. Quad. Geofis. 16, 185–186.

Lawver, L.A., Gahagan, L.M., 2003. Evolution of Cenozoic seaways in the circum-Antarctic region. Palaeogeogr. Palaeoclimatol. Palaeoecol. (this issue) 10.1016/S0031-0182(03)00392-4.

Lear, C.H., Elderfield, H., Wilson, P.A., 2000. Cenozoic deep-sea temperatures and global ice volumes from Mg/Ca in benthic foraminiferal calcite. Science 287, 269–272.

Lowrie, W., 1990. Identification of ferromagnetic minerals in a rock by coercivity and unblocking temperature properties. Geophys. Res. Lett. 17, 159–162.

Marks, K.M., Stock, J.M., Quinn, K.J., 1999. Evolution of the Australian-Antarctic discordance since Miocene time. J. Geophys. Res. 104, 4967–4981.

McKelvey, B.C., Hambrey, M.J., Harwood, D.M., Mabin, M.C.G., Webb, P.-N., Whitehead, J.M., 2001. The Pagodroma Group – a Cenozoic record of the East Antarctic ice sheet in the northern Prince Charles Mountains. Antarct. Sci. 13, 455–468.

Macphail, M.K., Truswell, E.M., submitted. Palynological analysis of core catcher samples, Hole 1166A, Prydz Bay, East Anarctica. Part 1; 142.5–220.84 m; Part 2; 240.36–362.03 m. Submitted to the Aust. Geol. Surv. Organisation-AGSO.

Miller, K.G., Fairbanks, R.G., Mountain, G.S., 1987. Tertiary oxygen isotope synthesis, sea level history, and continental margin erosion. Paleoceanography 2, 1–19.

Miller, K.G., Wright, J.D., Fairbanks, R.G., 1991. Unlocking the ice house, eustasy and margin erosion. J. Geophys. Res. 96, 6829–6848.

Moriwaki, K., Yoshida, Y., Harwood, D.M., 1992. Cenozoic glacial history of Antarctica – a correlative synthesis. In: Yoshida, Y. et al. (Eds.), Recent Progress in Antarctic Earth Science. Terra Scientific Publishing Company, Tokyo, pp. 773–780.

O'Brien, P.E., Cooper, A.K., Richter, C. et al., 2001. Proc. ODP, Init. Rep., Vol. 188 (online). Available from World Wide Web: http://www-odp.tamu.edu/publications/188_IR/188ir.htm.

Prothero, D.R., 1994. The Eocene-Oligocene extinctions. Annu. Rev. Earth Planet. Sci. 22, 145–165.

Ramsay, A.T.S., Baldauf, J.G., 1999. A reassessment of the Southern Ocean biochronology. Geol. Soc. Lond. Mem. 18, 122 pp.

Roberts, A.P., 1995. Magnetic properties of sedimentary greigite (Fe_3S_4). Earth Planet. Sci. Lett. 134, 227–236.

Royer, J.Y., Rollet, N., 1997. Plate-tectonic setting of the Tasmanian region. Aust. J. Earth Sci. 44, 543–560.

Sagnotti, L., Winkler, A., 1999. Rock magnetism and palaeomagnetism of greigite-bearing mudstones in the Italian peninsula. Earth Planet. Sci. Lett. 165, 67–80.

Shackleton, N.J., Kennett, J.P., 1975. Paleotemperature history of the Cenozoic and initiation of Antarctic glaciation: oxygen and carbon isotopic analyses in DSDP Sites 277, 279, and 281. Init. Rep. DSDP 29, 743–755.

Shipboard Scientific Party, 2001a. Explanatory notes. In: O'Brien, P.E., Cooper, A.K., Richter, C. et al.(Eds.), Proc. ODP, Init. Rep., Vol. 188, pp. 1–191 (CD-ROM). Available

from: Ocean Drilling Program, Texas A&M University, College Station, TX 77845-9547, USA.

Shipboard Scientific Party, 2001b. Site 1166. In: O'Brien, P.E., Cooper, A.K., Richter, C. et al. (Eds.), Proc. ODP, Init. Rep., Vol. 188, pp. 1–191 (CD-ROM). Available from: Ocean Drilling Program, Texas A&M University, College Station, TX 77845-9547, USA.

Schlich, R., Wise Jr., S.W. et al., 1989. Proc. ODP, Init. Rep., Vol. 120. Ocean Drilling Program, College Station, TX.

Snowball, I.F., 1997. Gyroremanent magnetization and the magnetic properties of greigite-bearing clays in southern Sweden. Geophys. J. Int. 129, 624–636.

Stagg, H.M.J., 1985. The structure and origin of Prydz Bay and MacRobertson Shelf. East-Antarct. Tectonophys. 114, 315–340.

Stephenson, A., 1980. Gyromagnetism and the remanence acquired by a rotating rock in an alternating field. Nature 284, 48–49.

Stephenson, A., 1981. Gyroremanent magnetization in a weakly anisotropic rock sample. Phys. Earth Planet. Inter. 25, 163–166.

Truswell, E.M., Macphail, M.K., 2001. Palynology of Cenozoic and Mesozoic sequences on the East Antarctic continental margin – a review. In: Florindo, F., Cooper, A.K. (Eds.), The Geologic Record of the Antarctic Ice Sheet from Drilling, Coring and Seismic Studies, Extended Abstract Volume for the Int. ANTOSTRAT Symp. Quad. Geofis. 16, 185–186.

Verosub, K.L., 1977. Depositional and postdepositional processes in the magnetization of sediments. Rev. Geophys. Space Phys. 15, 129–143.

Webb, P.-N., Harwood, D.M., 1991. Late Cenozoic glacial history of the Ross Sea embayment. Quat. Sci. Rev. 10, 215–223.

Weeks, R.J., Roberts, A.P., Verosub, K.L., Okada, M., Dubuisson, G.J., 1995. Magnetostratigraphy of Upper Cenozoic sediments from Leg 145, North Pacific Ocean. Rea, D.K. et al. (Eds.), Proc. ODP, Sci. Res., Vol. 145. Ocean Drilling Program, College Station, TX, pp. 491–521.

Whalen, P.A., Lazarus, D., 2001. Radiolarian biostratigraphy of Site 1165, ODP Leg 188, Antarctic margin near Prydz Bay. In: Florindo, F., Cooper, A.K. (Eds.), The Geologic Record of the Antarctic Ice Sheet from Drilling, Coring and Seismic Studies, Extended Abstract Volume for the Int. ANTOSTRAT Symp. Quad. Geofis. 16, 13–15.

Whalen, P.A., Lazarus, D., submitted. Radiolarian biostratigraphy of Site 1165, Prydz Bay, Antarctica. J. Micropal.

Whitehead, J.M., Bohaty, S.M., Quaternary-Pliocene diatom biostratigraphy of Prydz Bay (ODP Leg 188, sites 1165 and 1166), In: Florindo, F., Cooper, A.K. (Eds.), The Geologic Record of the Antarctic Ice Sheet from Drilling, Coring and Seismic Studies, Extended Abstract Volume for the Int. ANTOSTRAT Symp. Quad. Geofis. 16, 195.

Whitehead, J.M., McKelvey, B.C., in press. Cenozoic glacigene sedimentation and erosion at the Menzies Range, southern Prince Charles Mountains, Antarctica. J. Glaciol.

Whitehead, J.M., McKelvey, B., McMinn, A., 2000. 1997/1998 Cenozoic geological fieldwork in the Southern Prince Charles Mountains of East Antarctica. Terra Ant. 7, 655–656.

Wilson, G.S., 1995. The Neogene East Antarctic ice sheet: a dynamic or stable feature? Quat. Sci. Rev. 14, 101–123.

Wilson, G.S., Florindo, F., Sagnotti, L., Verosub, K.L., Roberts, A.P., 2000. Magnetostratigraphy of Oligocene–Miocene glaciomarine strata from CRP-2/2A, Victoria Land Basin. Antarct. Terra Ant. 7, 631–646.

Winter, D.M., Harwood, D.M., 1997. Integrated diatom biostratigraphy of Late Neogene drillholes in Southern Victoria Land and correlation to Southern Ocean records. In: Ricci, C.A. (Ed.), The Antarctic Region: Geological Evolution and Processes. Proc. VII Int. Symp. on Antarctic Earth Sciences. Terra Ant. Publ., pp. 985–992.

Winter, D.M., Iwai, M., 2002. Data report: Neogene diatom biostratigraphy, Antarctic Peninsula Pacific margin, ODP Leg 178 rise sites. In Barker, P.F., Camerlenghi, A., Acton, G.D., Ramsay, A.T.S. (Eds.), Proc. ODP, Sci. Res., Vol. 178 (online). Available from World Wide Web: http://www-odp.tamu.edu/publications/178_SR/chap_29/chap_29.htm.

Wise Jr., S.W., Schlich, R. et al., 1992. Proc. ODP, Sci. Res., Vol. 120. Ocean Drilling Program, College Station, TX.

Wright, J.D., Miller, K.G., 1992. Southern Ocean influences on late Eocene to Miocene deepwater circulation. In: Kennett, J.P., Warnke, D.A. (Eds.), The Antarctic Paleoenvironment: A Perspective on Global Change. Am. Geophys. Union Ant. Res. Ser. 60, 1–25.

Yanagisawa, Y., Akiba, F., 1998. Refined Neogene diatom biostratigraphy for the northwest Pacific around Japan, with an introduction of code numbers for selected diatom biohorizons. The Journal of the Geological Society of Japan 104 (6), 395–414.

Zachos, J., Pagani, M., Sloan, L., Thomas, E., Billups, K., 2001. Trends, rhythms, and aberrations in global climate 65 Ma to present. Science 292, 686–693.

Zielinski, U., Gersonde, R., 2002. Plio-Pleistocene diatom biostratigraphy from ODP Leg 177, Atlantic sector of the Southern Ocean. Mar. Micropal. 45, 225–268.